UNIVERSITÀ POLITECNICA DELLE MARCHE

DEPARTMENT OF ENGINEERING

Master's Degree in Biomedical Engineering

RESPIRATION ASSESSMENT FROM ELECTROCARDIOGRAM: AN EXPERIMENTAL STUDY

Advisor:

Prof. **Laura Burattini**

Co-Advisor:

Dr. **Agnese Sbrollini**

Dr. **Ilaria Marcantoni**

Candidate:

Tamara Lunghi

A.Y. 2021 / 2022

Abstract

The respiratory signal (RS) is one of the major markers to evaluate the state of health of a patient. Direct techniques are currently employed in the clinical context to assess RS. Nevertheless, direct monitoring may result uncomfortable for the patient, or hard to manage. As a result, indirect measurements of RS have been proposed through the years.

Among the many alternatives, one relies on the extraction of the RS from the electrocardiogram (ECG), defining the Electrocardiogram-Derived-Respiration (EDR). In fact, respiration is known to modulate ECG, since the respiratory and cardiac systems work together to ensure oxygen perfusion, in a way that any alteration in one system can be perceived in the other too. Hence, by analyzing this modulation, one can retrieve the RS. EDR has been usually characterized in terms of Breath-to-Breath (BB) interval. However, BB measurements are not always reliable. In fact, there is the chance that, even though the BB interval reflects a normal respiration pattern, the actual depth of the breath may be insufficient for a physiological respiration, in a way that the oxygen circulation would be insufficient as well. When such conditions occur, a major consequence is hypoxia, that in turn may lead to cerebral damages. As a consequence, other features for EDR characterization and classification have been investigated to obtain a reliable RS.

The aim of this study is to characterize EDR in terms of amplitude. 12-lead ECG data were acquired at the Cardiovascular Bioengineering Laboratory at Università Politecnica delle Marche (Ancona, Italy) on 50 subjects, each of whom performed different types of respirations, including apnea, deep respiration and normal respiration. Data were analyzed in MATLAB environment. In the very beginning, the raw ECG, which is modulated by respiration, has been filtered to remove the noise. Afterwards, the EDR for each type of respiration was obtained by using a modified version of the Segmented-Beat-Modulation-Method (SBMM), by computing EDR as the difference between the raw ECG, which is modulated by respiration, and the filtered non-modulated ECG, obtained as an output from the modified SBMM (mSBMM). The amplitude of EDR has been estimated by using three different methods: the difference between the maximum and minimum of the signal, four times the standard deviation of the signal, and the interquartile range, respectively. The accuracy in estimating the respiratory patterns has been assessed by using a statistical test, such as the Wilcoxon paired signed rank test, by setting the statistical significance at 0.05. Moreover, the diagnostic power of EDR amplitude has been quantified by measuring the area under the receiver operating characteristic curve. All the three methods led to statistically significant results, especially

when comparing deep respiration either to apnea or normal respiration. In particular, significant results have been obtained in all 12 ECG leads either in the case 'deep respiration vs apnea' or 'deep respiration vs normal respiration'. In fact, the median amplitude of deep respiration always resulted to be greater than the one of normal respiration or apnea. Considering the classification of apnea with respect to normal respiration, still significant outcomes were obtained, even though some leads provided non-statistically significant results. Indeed, in some leads the median EDR amplitude of apnea was much lower than the one from normal respiration, giving statistically significant results. However, in other leads this difference in amplitude was very small, or even it happened that apnea had a greater amplitude than normal respiration, leading to non-statistically significant results. The diagnostic power of the first method showed to be the best one, whereas the third method was hardly able to discriminate between different types of respiration. The reason why the first method came up as the best one lies in the way the signal was preprocessed. Indeed, in this study a preprocessing stage was carried out. Hence, if this study is to be applied to raw data, other methods should be employed to characterize EDR amplitude. On the other hand, the second method provided very accurate results, while the third one led to the least accurate outcomes. Hence, a suitable choice to characterize EDR amplitude could be the second method, which can be efficiently applied also to noisy data.

In conclusion, this study suggests that EDR characterization in terms of amplitude is a valid tool to classify RS, hence it is an efficient alternative to BB interval measurements. Nevertheless, future studies could be conducted in order to better analyze the effects of apnea on ECG modulation, when compared to normal respiration.

Contents

INTRODUCTION

The respiratory signal (RS) is a major factor in the determination of respiratory diseases. However, standard techniques may not always be applied in a clinical context. In fact, a direct measurement of the RS may be too uncomfortable, as in the case of the complex equipment when undergoing a nocturnal polysomnography, or even hard to manage in a clinical context, as it is for spirographic records. For these reasons, in the recent years many algorithms have been proposed trying to indirectly extract RS.

Among the many proposed alternatives, one comes from the electrocardiographic (ECG) signal. As a matter of fact, the cardiac and respiratory systems work together to ensure oxygen perfusion to the whole body, hence any alteration in either one of the two systems can be perceived in the other too. The RS which is obtained from the ECG is referred to as Electrocardiogram-Derived Respiration (EDR). In this way, it is possible to obtain a reliable and continuous RS, simply by measuring the cardiac electrical activity, without being much invasive to the patient.

Normally, EDR is characterized in terms of breath-to-breath (BB) interval, and many algorithms have been proposed in the recent years. However, BB measurements are not always reliable. In fact, there is the chance that, even though the BB interval reflects a normal respiration pattern, the actual depth of the breath may be insufficient for a physiological respiration, hence the oxygen circulation would be insufficient as well. When such conditions occur, a major consequence is hypoxia, that in turn may lead do cerebral damages. As a result, other features for EDR characterization have been investigated to extract a reliable RS.

The aim of this study is to characterize EDR in terms of amplitude, by using a new procedure based on a modified version of the Segmented-Beat Modulation Method (mSBMM) [1] [2]. The idea is to characterize EDR starting from a series of ECG data acquired while simulating different types of respiration, especially apnea, deep respiration and normal respiration. Later, EDR is extracted and characterized in terms of amplitude.

1 THE RESPIRATORY SYSTEM

The respiratory system is made of a group of hollow organs, the airways, and two parenchymatous organs, the lungs. Airways are the channels that bring air from the outside to the lungs. Lungs are the sites in which oxygen and carbon dioxide are exchanged. Hence, from a functional and anatomical standpoint, the respiratory system is highly correlated with the cardiovascular system [3].

Respiration is a complex process that relies heavily on the coordinated action of the muscles of respiration and the control center in the brain. Respiration must always be ensured, since oxygen is critical for proper metabolism on a cellular level, while carbon dioxide is crucial for achieving adequate pH levels. Several mechanisms exist to ensure a rigorous balance between supply and demand. In response to a change in blood gases, the pulmonary system adapts by adjusting respiratory patterns to meet the body's metabolic demand.

The respiratory function is carried out in two phases, the inspiration and the expiration. During inspiration, the air full of oxygen, which comes from the external environment, reaches the lungs via the airways. During expiration, the air, full of carbon dioxide, travels back via the airways and is expelled to the external environment [3].

1.1 ANATOMY OF THE RESPIRATORY SYSTEM

The airways are the channels that bring air from the outside to the lungs. Airways consist of nose, pharynx, larynx, trachea, and bronchi (Fig. 1) [3].

The bridge of the nose includes the external nose and the nasal cavities.
The external nose has a triangular pyramidal form and has three faces: two lateral and an inferior. The inferior face is characterized by two orifices, the nostrils.
The nasal cavities are large spaces in the middle of the face, and are divided by a median septum, that is the nasal septum. They communicate with the external environment and the larynx, respectively, via the nostrils and the choanae.
The nasal cavities are internally coated with the respiratory mucosa. Its main function is to prevent pathogens and noxious particles from reaching the lungs. The nasal mucosa also warms the air to

near body temperature. The nasal cavities are also characterized by the olfactory mucosa, which includes the olfactory cells. These cells are modified neurons which have specialized cilia extension. The cilia capture odor stimuli from molecules that enter the cavities [3].

From the nasal cavity air passes to the pharynx. It is a hollow tube that goes from the cranial base to the 6th cervical vertebra, where it continues with the esophagus.
The pharynx is a channel in common to the respiratory and the digestive systems, thus it allows the passage of air and food.
The pharynx can be divided into 3 consecutive parts: the nasopharynx, the oropharynx, and the laryngopharynx [3].

Then the air passes to the larynx, placed between the pharynx and the trachea. The larynx is formed by different cartilage: thyroid, epiglottic, cricoid, arytenoid and corniculate. The epiglottic cartilage is very important. In fact, it closes during swallowing, thus closing the access to the larynx [4].

Beyond respiratory function, the larynx contains the vocal cords and is essential to human speech. In fact, the larynx has different membranes, including the quadrangular and the elastic one. From the margins of these membranes, the fibrous skeletons of the false and true vocal cords are formed. The true vocal cords demarcate a triangular opening, the rima glottidis. The larynx muscles allow movement of the rima glottidis: during breathing this inlet is open, but it closes during speech, allowing phonation [3].

The trachea follows the larynx and at the level of the mediastinum It bifurcates into the two main bronchi, which are directed towards the lungs. The trachea is made of 15-20 cartilage rings, which are connected via fibrous laminae called annular ligaments [3].

The main bronchi originate from the larynx. The bronchi are two large tubes that carry air to the lungs, and their walls are made of four layers, one overlapping the other.
Each of the two extrapulmonary bronchi reaches the respective lung hilum, where they arborize in intrapulmonary bronchi penetrating the lungs [3].

The lungs are placed in the thoracic cavity and separated by the mediastinum. They are wrapped in a serous membrane, the pleura, consisting of two layers. In the thin space between the two layers, called the pleural cavity, there is a negative pressure that allows the lungs to expand during inspiration. Moreover, in the pleural cavity there is the pleural fluid, that facilitates the sliding of the

lungs during the respiration.

The lungs have a conic shape with a superior apex; their bases face the diaphragm and are concave. The medial, or mediastinal, face is constituted by the hilum, which is entry site of the main bronchi and blood vessels. The right lung is larger than the left one; as a matter of fact, the thoracic cavity also houses the heart. As a result, since the heart protrudes to the left, the left lung has less space than the right one, and is thus smaller. The right lung is divided in three lobes, while the left one, being smaller, is only divided into two lobes [3].

As soon as the bronchi enter the lungs, they arborize, giving rise to the bronchial tree, in a way that the bronchi arborize. These branches will divide the lungs into pulmonary lobules. These form the pulmonary parenchyma. Every lobule receives a lobular bronchus, which in turn branches into intralobular bronchia and then terminal bronchia. The terminal bronchia bifurcate in two respiratory bronchioles, whose walls are constituted by a capillary network originating from the branches of the pulmonary artery. This network are the pulmonary alveoli, where the gas exchanges occur [4].

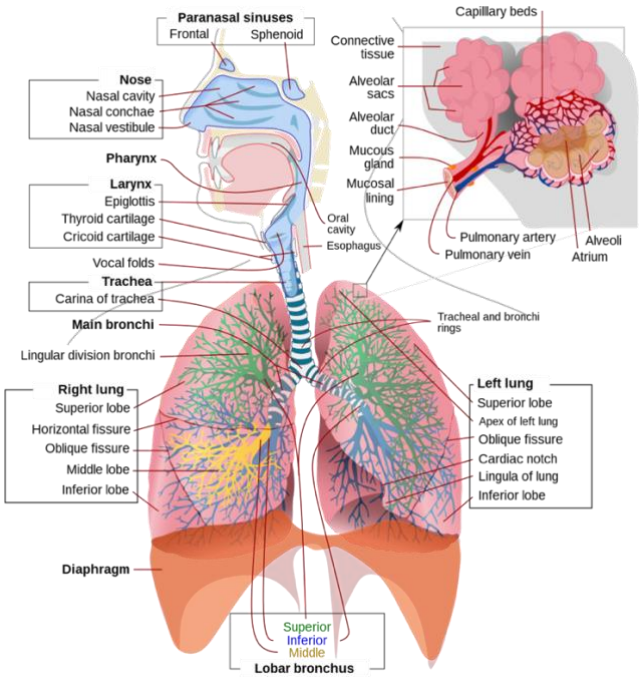

Figure 1. The respiratory system

1.2 PHYSIOLOGY OF THE RESPIRATORY SYSTEM

1.2.1 Respiration

The respiration is governed by diffusion, a phenomenon by which molecules move from areas of high concentration to areas of low concentration across a barrier. In particular, there is the diffusion of oxygen O2 from the alveoli to the pulmonary-capillary blood, and the movement of CO2 in the opposite direction. Diffusion is governed by Fick's law, which can be simplified as in equation (1):

$$\dot{V} = D_L \cdot (P_1 - P_2) \tag{1}$$

where $\dot{V}$ is the flow of gas, D_L is the diffusing capacity of the lungs, and P_1 and P_2 are, respectively, the pressures in the two sites at the barrier (Fig. 2).

D_L is depending on the area and thickness of the barrier, but also on the molecular weight (MW) and solubility of the gas involved in the diffusion. As a result, equation (1) becomes:

$$\dot{V} = \left(k \frac{A \cdot s}{a \sqrt{MW}}\right) \cdot (P_1 - P_2) \tag{2}$$

where k is a diffusion constant, A is the area of the barrier, s represents the gas solubility, a is the thickness of the barrier, and finally MW is the molecular weight of the gas [5].

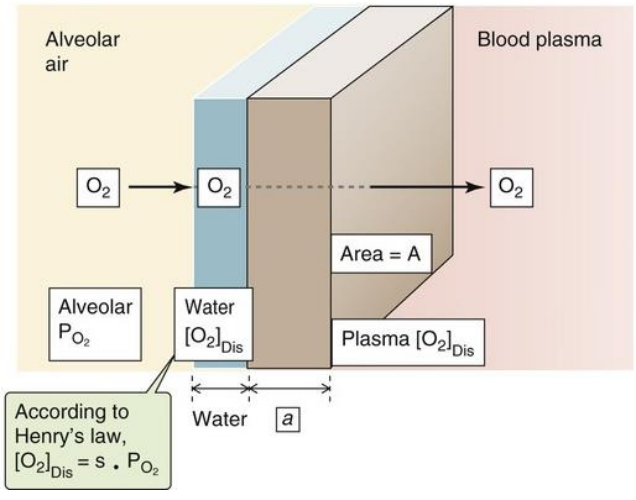

Figure 2. Diffusion of gas across the alveolar wall [5].

Although diffusion is the main ruler of respiration, two other important parameters must be underlined: ventilation and perfusion. These two are very important because they set up the partial pressure gradients along which O2 and CO2 diffuse. Ventilation is the convective movement of air that exchanges gases between the atmosphere and the alveoli, while perfusion is the convective movement of blood that carries the dissolved gases to and from the lung.
The V/Q ratio is the ratio between the ventilation and perfusion, and it is used to check if the two processes are working properly. If, for instance, the ventilation reduces, alveolar gas exchange will be impaired. Hence, the arterial blood cannot be properly oxygenated, in a way that the capillary partial pressure of oxygen (pO2) will fall, and the partial pressure of carbon dioxide (pCO2) will rise [5].

As said earlier, thanks to diffusion, oxygen moves from areas of high concentration to areas of low concentration. In particular, it diffuses through the alveolar wall and goes to the blood and plasma, contained in the capillaries in the lungs, where it binds to a protein, hemoglobin. As a result, this protein gets oxygenated and becomes oxyhemoglobin. Then, the oxygenated blood will be sent to the left heart and then to all the body, to oxygenate all the body tissue.
On the other hand, CO2 moves from an area of high concentration, as it is blood coming from the right heart to an area of low concentration, the alveoli. Then, by travelling through the airways, CO2 will be expelled [6].

This exchange mechanisms at alveolar and capillary levels occur thanks to mechanical movements of the lungs and the surrounding muscles.
The lungs contain 2-300 million alveoli, with a total surface area, for gas exchange, of approximately 140 m^2. For an ordinary breath, the average velocity of gas in the trachea is around 0.7 m/ s, but at the alveolar surface it is no higher than 0.001 m/ s. In the following, some lung parameters are reported:

- Total lung capacity (TLC, L): the gas volume in the lung after a maximum inspiration (typically 6-8 L)
- Residual volume (RV, L): the remaining gas volume after an expiration (around 4-6 L)
- Vital capacity (VC, L): the maximum volume that can be inspired (normally 3-4 L) [6].

The interaction between the lungs and the thoracic cage determines the lung volume. The lungs tend to collapse because of their elastic recoil, that is an intrinsic tendency to deflate following inflation. The chest wall has elastic recoil too.

The lungs' elastic recoil tends to pull the thoracic cage outward, while the chest wall recoil pushes the lung inward. This interaction between lungs and chest wall does not occur by direct attachment, but via the intrapleural space, characterized by an intrapleural pressure (PiP). At equilibrium, the inward action of the chest wall balances the opposite action of the lungs, resulting in a negative PiP of about -5 cmH20 and expanded lungs (Fig. 3) [5].

The lung expandability is usually measured in terms of compliance, which is described as the change in lung volume (ΔV) because of pressure changes (ΔP) in the lung. Compliance can be computed as it follows [7]:

$$C = \frac{\Delta V}{\Delta P} \tag{3}$$

Any change in the balanced action of chest wall and lungs leads to a change in lung volume. The different phases of respiration, inspiration and expiration, are in fact governed by modulation of the elastic recoil of the chest walls, which is driven in turn by changes in tension of the respiration muscles. During inspiration air is inflated and reaches the lungs, while during expiration air is expelled in the outside environment. During inspiration, the chest is expanded, and thus the elastic recoil of the chest wall does. This makes the PiP more negative. As a consequence of the expansion of the chest, the lungs expand passively. The muscles that produce a quiet inspiration are called the primary muscle of inspiration and include the diaphragm and some intercostal muscles, most being external intercostal muscles. During a forced inspiration, the accessory muscles are involved, in addition to the aforementioned muscles. The accessory muscles include scalenes, sternocleidomastoids, neck and back muscles and the upper respiratory tracts [5].

During a quiet expiration, the intrapleural pressure becomes less negative and no muscles are directly involved. As a matter of fact, the lungs have simply stored enough energy in their elastic recoil to fuel a quiet expiration, making the expiration a passive action. Hence, during a quiet expiration, it is simply the respiration muscles that relax, and no primary muscles of expiration exist. Nevertheless, during a forced expiration, some muscles are involved, as now expiration is not completely passive. In this case, some accessory muscles of expiration help to make the PiP less negative, including abdominal muscles, intercostals, neck and back muscles (Fig. 4).

Beyond normal respiration, which is also called eupnea, other types of respiration exist, including apnea, orthopnea and many others.

For instance, apnea is the cessation of respiration: the respiratory muscles do not move, and the lung volume remains unchanged. Apnea can be either forced, when one spontaneously holds his breath, or it can be involuntarily, for instance during sleep [8].

On the other hand, orthopnea is defined as the sensation of breathlessness in the recumbent position relieved by sitting or standing.

Moreover, it is also possible to perform deep respiration, consisting in inspirating as much air as possible to fully fill the lungs. During deep breath, also called diaphragmatic respiration, the lower belly rises [9].

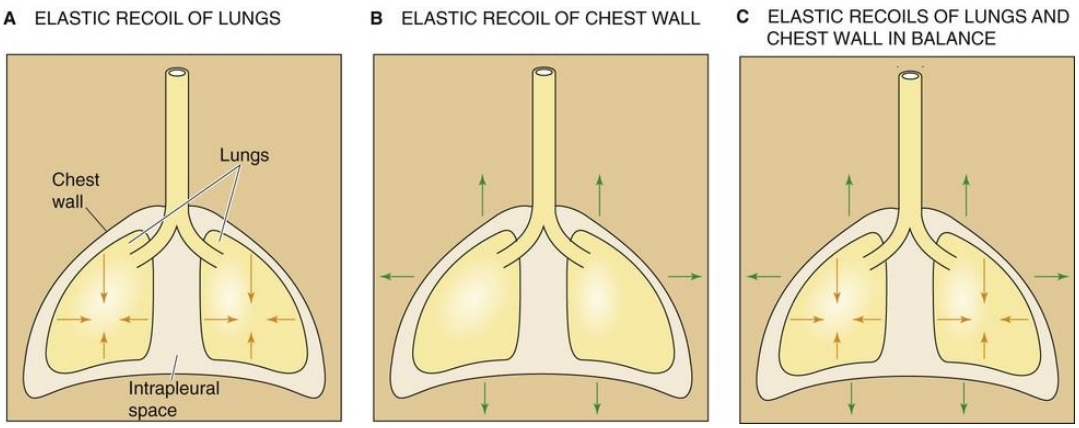

Figure 3. Elastic recoil of lungs and chest wall [5].

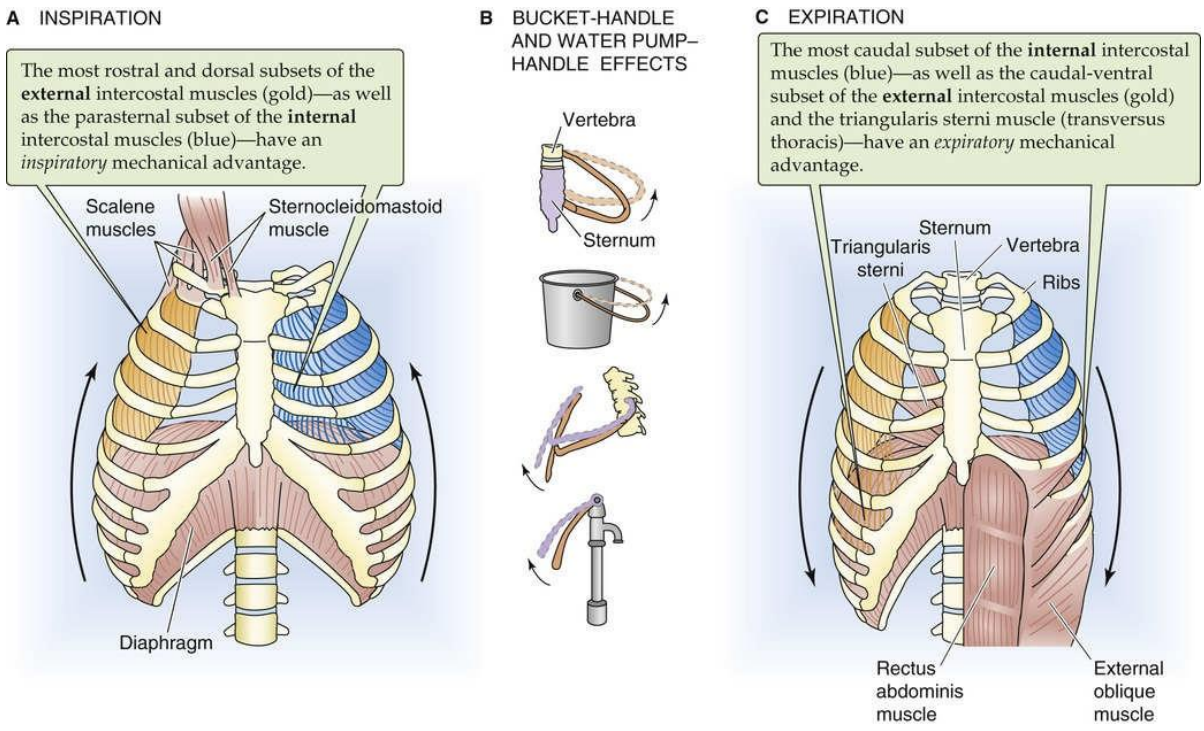

Figure 4. Inspiration and Expiration [5].

1.2.2 Respiratory signal

There are several methods for measuring and monitoring respiration.

One of the possible techniques is the spirographic signal. A spirometer measures the volume of air that is inspired and expired; hence it measures the change in lung volume. Fig. 5 shows a typical spirographic record. The inspiration-expiration couple mechanism is represented as a sinusoidal wave, where the growing part of the curve represents the inspiration, while the descending part is the expiration. The most important respiration parameters are reported in the following:

- Tidal volume (TV, L): the amount of air entering and leaving the lungs with each breath. During quiet expiration, it is approximately 500 mL.
- Total ventilation (TVE): it is the product of TV and the frequency of breaths, and it is given in liters per minute.
- Expired lung volume (VE, L): the leaving air volume.
- Inspiratory reserve volume (IRV, L): it is the additional volume of air that the subject could inhale with a maximal effort after a quiet inspiration.

The magnitude of IRV depends on many factors, including the current lung volume. As a matter of fact, the greater the lung volume after the inspiration, the smaller the IRV will be. Other factors that influence IRV are the lung compliance (the easier the expandability of the lung, the more the IRV will be), muscle strength (the stronger the muscle, the more the IRV), comfort, flexibility of the skeleton and posture. On the other hand, the amount of volume that the subject can expel with a maximal effort, after a quiet expiration, is called expiratory reserve volume (ERV), and depends on the same factors as IRV. It must be underlined that, even after a maximal expiratory effort, some air remains inside the lungs: it is the RV [5].

Lung capacity can be determined as the combination of lung volumes.
The TLC is defined as the sum of the four lung volumes. The functional residual capacity (FRC) is the sum of ERV and RV, and it represents the amount of air that remains in the lung after a quiet expiration. The inspiratory capacity (IC) is the sum of TV and IRV. It is the maximal amount of air a person can inspire after a quiet expiration. Finally, the VC is the sum of IRV, ERV and TV. VC represents the maximal achievable TV.

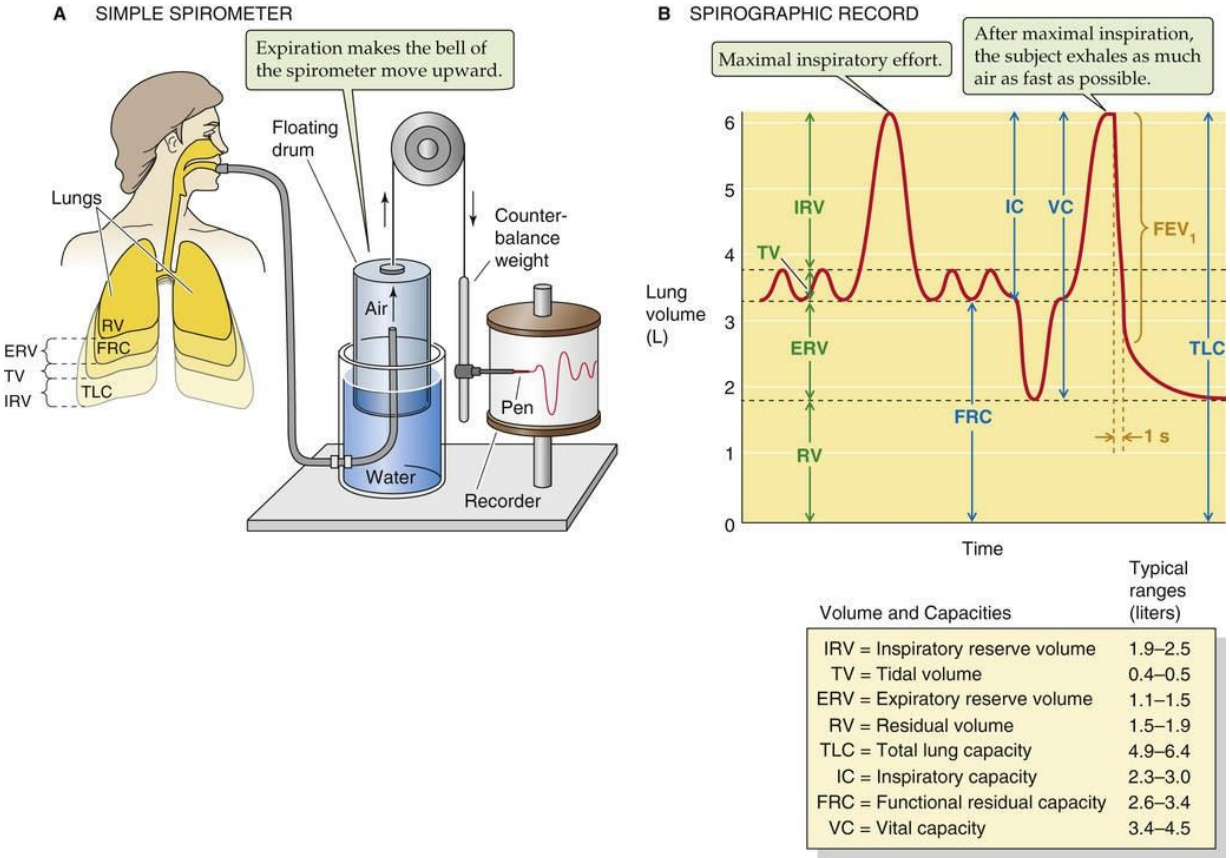

Figure 5. Spirographic record [5].

Methods other than spirometry are possible to monitor respiration. For instance, plethysmography is a technique which measures changes in volume in the lungs, usually by means of a respiratory belt. Three plethysmography techniques are currently implemented: elastomeric, impedance and respiratory induced (RI) plethysmography [10].

In elastomeric plethysmography, a belt with two or more sensors is worn by the patient around the chest or the abdomen. In this way, as soon as the chest or the abdomen moves, the belt will undergo a change in tension, which will be then converted to a voltage.
In particular, inhalation is represented as a downward trend in the respiratory waveform, because during inhalation the thoracic cavity is expanding, thus compressing the belt. As a consequence, the distance between the sensors in the belt decreases, and the signal decreases. On the other hand, expiration provokes a dilation of the belt, thus resulting in an increasing signal. There are many sensors that are able to convert tension in a voltage, even though the most used sensor is the piezo-electric crystal, which generates an electric signal when it is mechanically deformed.

Impedance plethysmography exploits the high impedance of the body. As the lungs vary their volume, the body impedance changes. In order to measure these changes, two or more electrodes are placed on the skin of the patient and are travelled by an alternating current. The impedance variations are in fact represented as a sine wave, with inward and upward deflections representing inspiration (increased impedance) and expiration (decreased impedance), as it was for the spirographic signal [11].

Finally, RI plethysmography is based on Faraday's law and Lenz's law. -
An alternating current is passed through the belt (that is a loop of wire), so that a magnetic field is generated, normal to the orientation of the loop (Faraday's law). Then, changes in the area of the belt (i.e., the area enclosed by the loop), caused by inspiration and expiration, create an opposing current within the loop directly proportional to the change in the area (Lenz's law). This opposing current can then be easily measured, as a change in the frequency of the applied current. An advantage of RI plethysmography is that, not relying on bel tension, it is not affected by belt trapping [10]. Depending on the site where the belt is placed, thoracic and abdominal respiration can be distinguished. During normal respiration, there is synchronous expansion of the chest and the abdomen. However, during pathological respiration, no synchronous expansion is present. In fact, airway obstruction can be detected by RI plethysmography due to a phase shift in thoracic (in the

chest) and abdominal expansions (Fig. 6) [12]. Fig. 7 and 8 represent RS coming from different types of respiration, respectively deep respiration, and apnea. The BB interval can be defined as the number of the respiration per minute. In eupnea the BB is between 12 and 20 breaths/min [5].

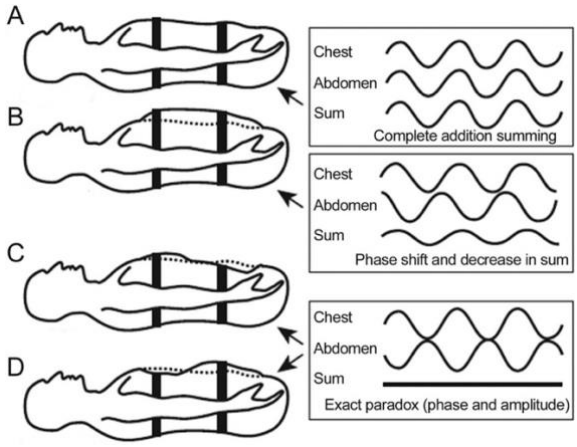

Figure 6. Normal breathing (A), phase shifting (B), and paradoxical breathing (C and D) as correlated to analog signal by respiratory inductance plethysmography [12].

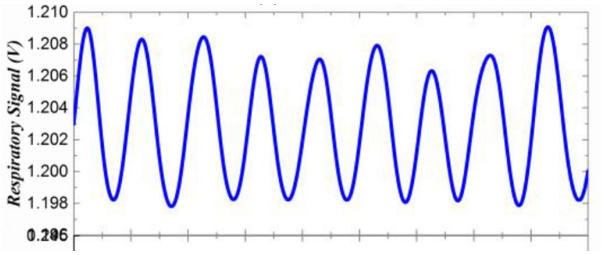

Figure 7. Deep respiration

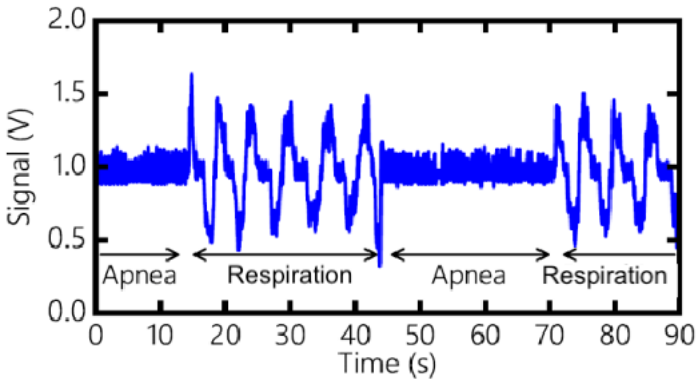

Figure 8. Normal respiration and apnea

2 THE CARDIOVASCULAR SYSTEM

The cardiovascular system has two primary components: the heart and blood vessels, which can be distinguished into arteries, veins, and capillaries (Fig. 9) [3].
The heart can be viewed functionally as two pumps with the pulmonary and systemic circulations situated between the two pumps. The pulmonary circulation is the blood flow within the lungs that is involved in the exchange of gases between the blood and alveoli. The systemic circulation is comprised of all the blood vessels within and outside of organs excluding the lungs [7].

2.1 ANATOMY OF THE HEART

The heart is located in the thoracic cavity, and it is contained in a connective sac, the pericardium. The heart is placed in the center of the thoracic cavity but protrudes more towards the left. On the inside, it is entirely covered with the serous pericardium. Going from inner to outer layer, there are endocardium, myocardium, and epicardium. The heart consists of four chambers: right atrium, right ventricle, left atrium and left ventricle. The walls of the chambers are filled with the muscle layer of the heart, the myocardium, which is made up of cardiac myocytes [3].

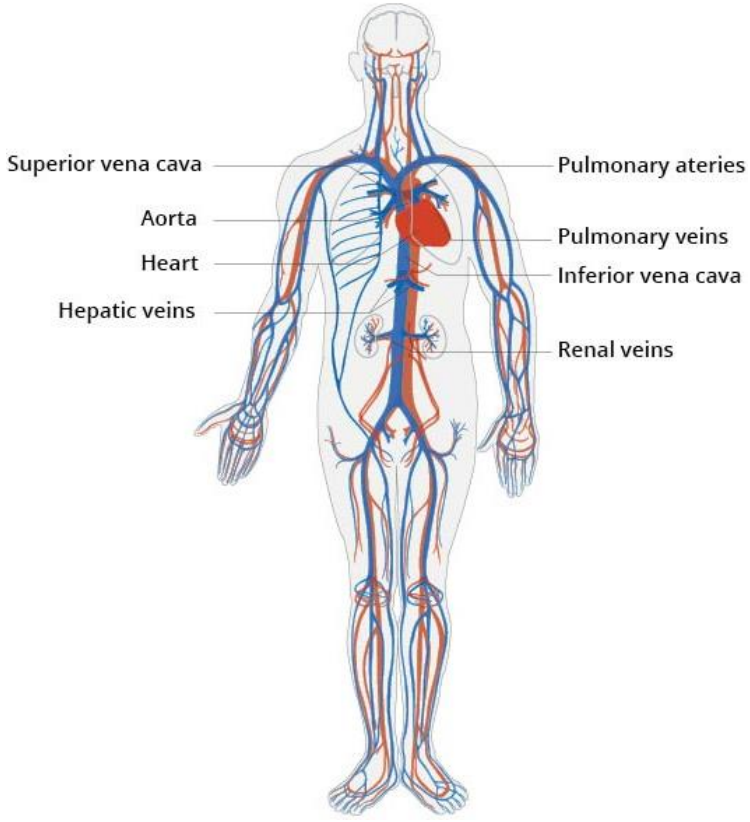

Figure 9. The cardiovascular system

Ventricles are thicker than atria, since they need to sustain higher blood pressure. Moreover, most of the cardiac muscle tissue is found in the left free ventricular wall. Hence, the left ventricle is thicker than the right one.

After birth, unless an abnormal development of the heart, no connection is possible between the two atria and between the two ventricles, thanks to the interatrial and interventricular septa. In the heart, there is also an atrioventricular ring, the fiber skeleton, which acts as an electrical insulator between the atria and the ventricles. The only connection between atrium and ventricle is via an atrio-ventricular orifice, provided with a valve. The tricuspid valve ensures blood flow from the right atrium to the right ventricle. In the same way, communication between the atrium and ventricle in the left part of the heart is achieved via the mitral valve. Both the tricuspid and mitral valves have fibrous strands (chordae tendineae) on their leaflets that attach to papillary muscles located on the respective ventricular walls. The papillary muscles contract when the ventricles contract, thus preventing backflow of blood towards the atria. Similarly, the connection between the ventricles and the arteries is guaranteed by orifices and valves. The semilunar valves give access to the main arteries, (pulmonary arteries and to the aorta), respectively from right ventricle (pulmonary valve) and from left ventricle (aortic valve), as shown in Fig. 10 [3], [7].

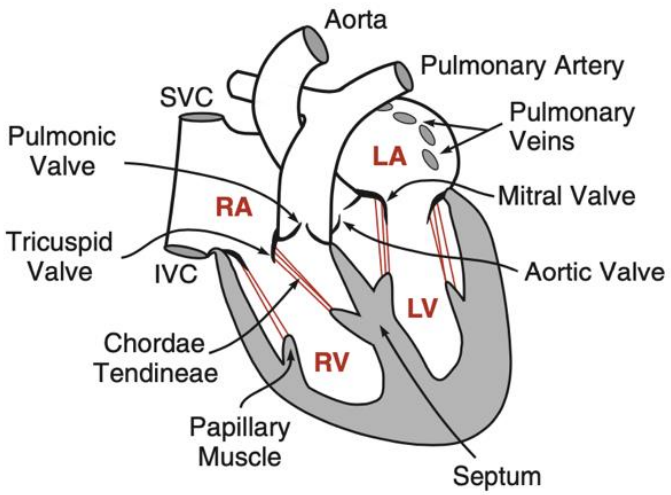

Figure 10. Anatomy of the heart [7].

2.2 CIRCULATION

The circulation delivers nutrients and oxygen to all cells in the body. It consists of the heart and different blood vessels, which can be divided into three major categories: arteries, veins, and capillaries.

There are two circulations which are connected through the heart. The pulmonary circulation moves blood between the heart and the lungs. It transports deoxygenated blood to the lungs to absorb oxygen and release carbon dioxide. The systemic circulation moves blood between the heart and the rest of the body; it provides organs, tissues, and cells with blood, so they get oxygen and other vital substances (Fig. 11).

Arteries carry blood away from the heart; veins carry it back to the heart. Capillaries allow nutrients and oxygen exchange at a tissue level [3].

The pulmonary circulation starts in the right atrium, which receives deoxygenated blood (or venous blood) from the superior and inferior vena cavae. The right atrium pumps the low-oxygen blood into the right ventricle. The right ventricle then ejects blood into the pulmonary artery, which branches off into smaller arteries and capillaries. At the level of the capillaries, the venous blood loses carbon dioxide and acquires oxygen, thus becoming oxygenated (also called arterial blood.)

From capillaries veins are formed.

The arterial blood is then transported to the left heart and enters the left atrium via the four pulmonary veins. This marks the end of the pulmonary circulation and the start of the systemic circulation. Now blood is pumped to the left ventricle, which in turn pumps it into the aorta, a big artery which bifurcates into the main arteries that perfuse all the body. The arteries eventually branch off into capillaries, where there is an exchange with interstitial fluid. In this way, cells acquire oxygen and nutrients and expel carbon dioxide, making the blood deoxygenated. The venous blood is then transported via veins to the right atrium [3], [7].

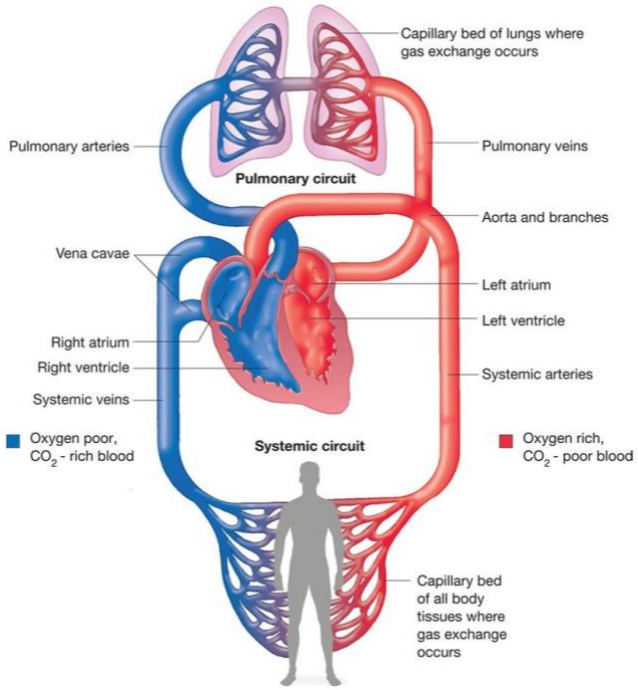

Figure 11. Blood circulatory system

2.3 ELECTROPHYSIOLOGY OF THE HEART

The heart is made of excitable cells, the cardiac myocytes. Myocytes can be distinguished into two categories:

1. pacemaker cells, that have spontaneous automaticity, hence can generate impulses
2. conducting cells, that can propagate the stimulus once they have received it through specific channels between the cells. This cardiac activity can be recorded at the skin of the patient.

2.3.1 Action potential

Cardiac myocytes are characterized by different ion concentrations and their respective channels, including sodium (Na^+), calcium (Ca^{2+}) and potassium (K^+). In particular, K^+ concentration outside the cell (4 mM) is way smaller than the inside one (150 mM). The opposite is true for Na^+ and Ca^{2+}, which have higher extracellular concentrations, being them respectively of 145 mM and 2.5 mM with respect to the intracellular ones (20 mM and 0.0001 mM).The relative intracellular and extracellular concentrations make up the membrane potential.

When the myocyte is at rest, it is in an equilibrium condition and its K+ channels are open, while the other channels are closed. In this equilibrium condition, the K+ outflow caused by diffusion forces is balanced by K+ inflow as a result of electrostatic forces and the resting membrane potential of the cell is around -90 mV. However, a stimulus can modify the potential and can give rise to a depolarization-repolarization phenomenon, known as action potential. The action potential is characterized by four phases, plus another phase during which the cell goes back to the resting state. During phase 0, in response to a stimulus, the membrane potential increases until a threshold around -65 mV is overcome. Phase 0 corresponds to a rapid depolarization, characterized by an increase in the conductance of the Na+ channels which open in turn, and closing of K+ channels. This allows Na+ ions to enter in the cell and leading to an increase in the membrane potential. After a short time, the Na+ channels close while some K+ channels open, leading to an early repolarization, that is phase 1. Phase 2 follows, during which Ca++ and K+ channels open, making respectively Ca++ to flow inside the cell and K+ outside the cell. Unlike Na+ channels, Ca++ channels remain open for a longer time, making phase 2 longer than phase 1. Phase 3 follows, during which the K+ conductance increases, while the Ca++ one decreases. As soon as the resting conditions are restored, phase 4 occurs. It is worth mentioning that during phases 0, 1 2 and part of 3, the cell is refractory and cannot generate any new action potentials. This is the effective (or absolute) refractory period (Fig. 12) [7].

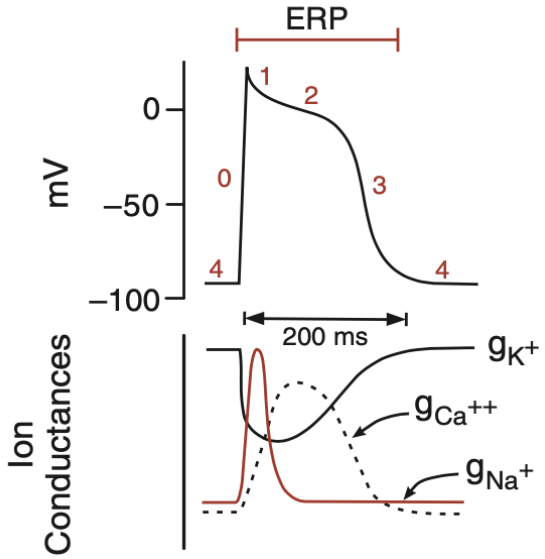

Figure 12. Action potential of a ventricular myocyte [7].

2.3.2 *Electrical conduction of the heart*

Once the stimulus has been generated by the pacemaker cells, the depolarization propagates from cell to cell throughout the right atrial muscle and, after some time, spreads to the left atrium. About one tenth of a second after its origination, the electrical signal arrives at the atrioventricular (AV) node. The impulse does not spread directly from the atria to the ventricles because of the presence of the fibrous skeleton. Instead, the only available pathway is for the impulse to travel from the AV node to the His-Purkinje fiber system, a network of specialized conducting cells that carry the signal to the muscle of both ventricles, namely at the apex of the heart. From there, the depolarization spreads across the whole ventricular muscles, so that approximately 200 ms after the onset of the stimulus in the SA node, all the heart is depolarized (Fig. 13). Fig. 14 shows the typical conduction pathways through the heart.

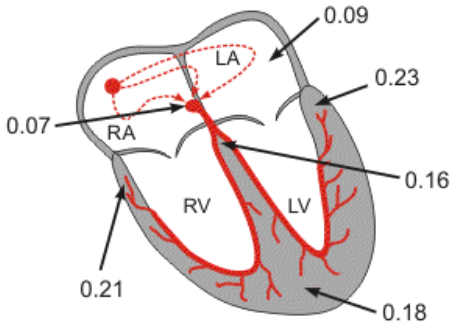

Figure 13. Cardiac activation times in the heart [7].

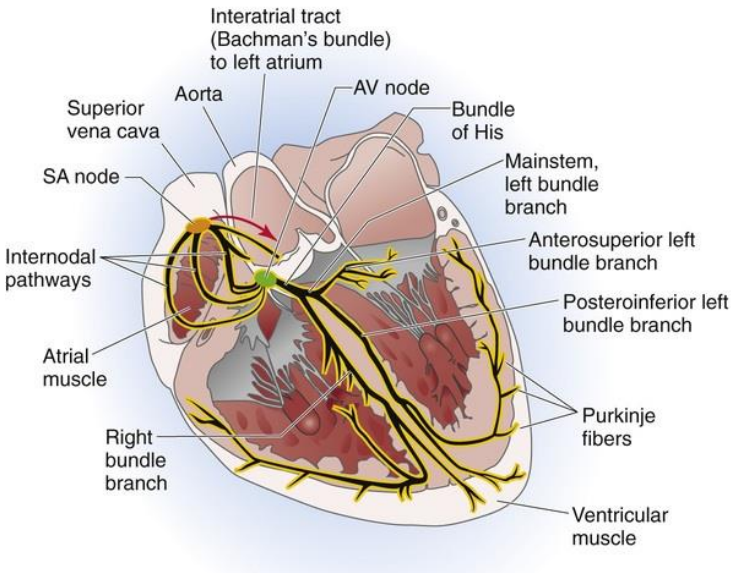

Figure 14. Conduction pathways through the heart [5].

2.4 MECHANOPHYSIOLOGY OF THE HEART

2.4.1 Cardiac Cycle

As anticipated earlier, the excitation of cardiac myocytes causes a depolarization, and, therefore, triggers contraction: this phenomenon is called excitation-contraction coupling. Hence, once the stimulus travels through a chamber, this will contract. To refer respectively to relaxation and contraction, the terms diastole and systole are used [5].

Before the stimulus is generated, the atria are passively and slowly filling. The atrial pressure is higher than the ventricular pressure. The AV valves are open, but low blood is flowing to the ventricles. Both atria and ventricles are relaxed, thus are in a diastolic stage. This stage is referred to as ventricular filling. As soon as the impulse is generated, the atrial cells depolarize and subsequently contract, thus increasing the atrial pressure against the ventricular pressure. Now the ventricles are filling, and the atria are emptying. This is the atrial systole. Up to now, the ventricles are still relaxed, thus they are in their diastolic stage. When the stimulus arrives at the AV node, it spreads among the ventricular myocytes, which in turn repolarize and contract. As soon as the contraction starts, the ventricular pressures increase. When the ventricular pressures exceed the atrial pressures, the AV valves close to avoid blood backflow to the atria. At this point, the atria are relaxing, and are in their diastolic stage, whereas the ventricles are contracting in an isovolumetric way. This phase is in fact called isovolumetric contraction. The ventricular pressures continue to increase. After a short time, the ventricular pressures will exceed the pressures of the pulmonary artery and aorta. Therefore, the semilunar valves open, allowing blood flow towards the major arteries. This stage is named ventricular ejection. After some time, the ventricular pressure will start decreasing. When these pressures will go back at values lower than the pressure of the two main arteries, the semilunar valves will close, and the ventricles will relax. Now, the ventricles are in the isovolumetric relaxation state. The ventricular pressures continue to decrease. When they will reach values lower than the atrial pressures, the AV valves will open, allowing blood flow from the atria to the ventricles, thus going back to a passive filling, that is the ventricular filling (Fig. 15) [5].

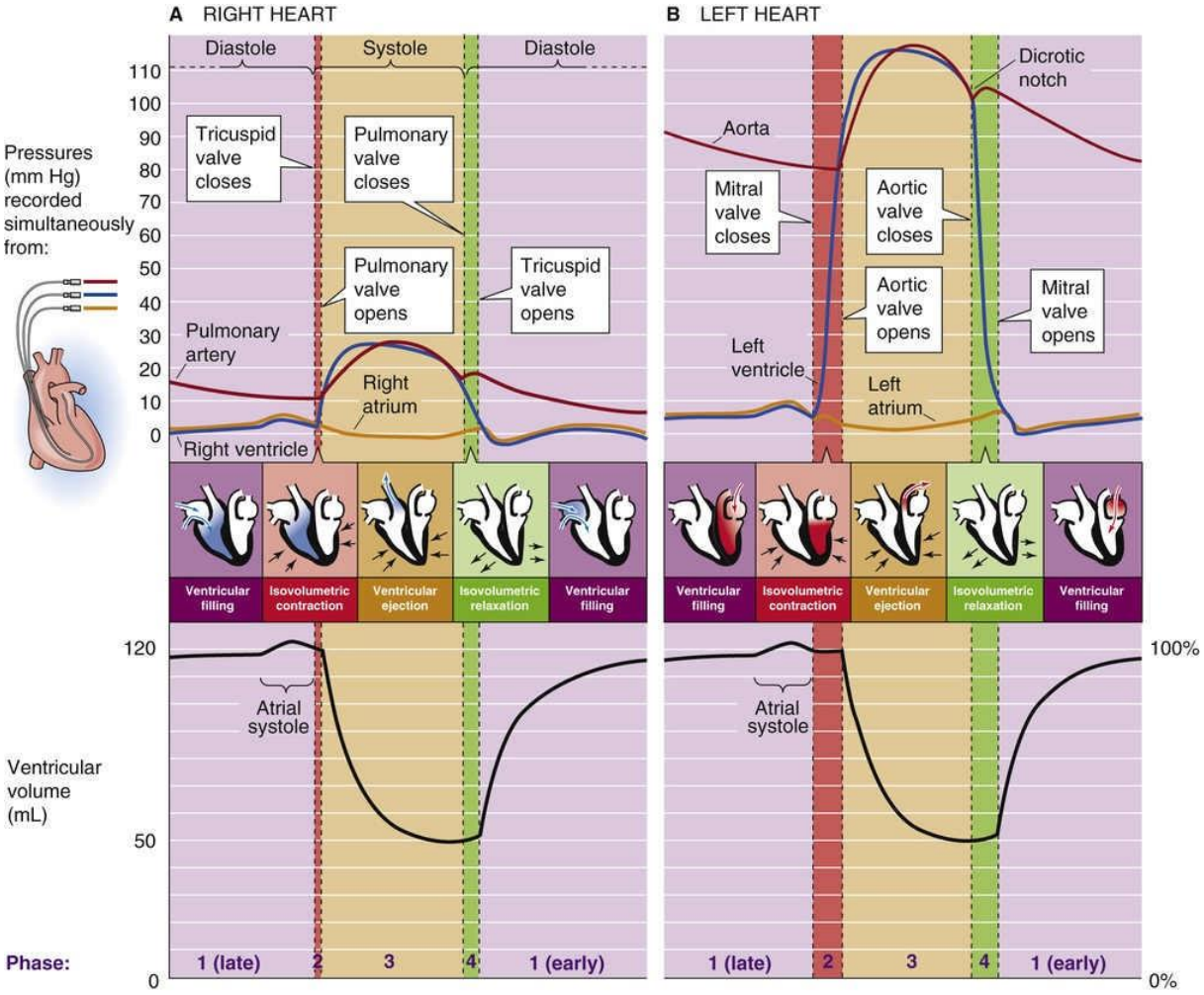

Figure 15. Pressures and volumes during the cardiac cycle [5].

2.5 ELECTROCARDIOGRAPHIC SIGNAL

The nerves and the muscle of the heart can be considered as a source of electrical charges across a conducting medium, that is the thorax. This electrical activity can be detected by means of electrodes placed at specific locations on the body surface. In fact, as cardiac cells depolarize and repolarize, electrical currents spread throughout the body, because the tissues surrounding the heart are able to conduct electrical currents. These currents produce an electric field, which emerges on the body surface with its equipotential lines. If electrodes are placed on the thoracic surface, on two lines of the field, a potential difference can be detected (Fig. 16). The recorded tracing is called ECG. Being the potential difference a function of depolarization and repolarization, it varies in time, resulting in ECG as a function of time [13].

Fig. 17 represents an instant in which all the cardiac myocytes in the heart are depolarized. As a result, equipotential lines will be generated. Three electrodes are placed over the thorax in different positions, respectively A, B and C, approximately at the vertices of an equilateral triangle.

It can be noticed that the potential difference depends on the electrode position. Moreover, it is observed that the shape of the equipotential lines can be obtained by considering two opposite electrical charges, which form a dipole [14].

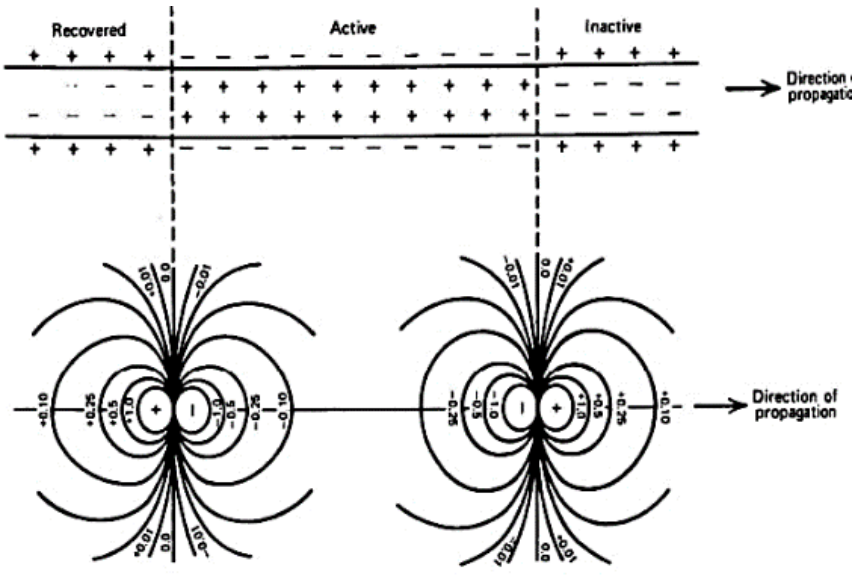

Figure 16. Electric field produced by the heart [14]

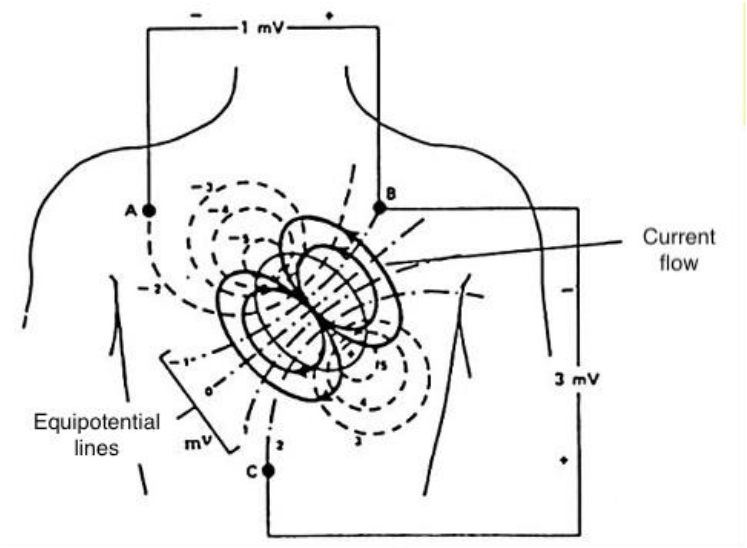

Figure 17. Equipotential lines during ventricular repolarization [14].

The potential difference generated by a charge *Q* at a certain distance *d* between the dipole and the electrode is defined as it follows:

$$E(d) = \frac{Q}{4\pi\varepsilon_0\varepsilon_r d} \tag{4}$$

with ε_0 being the absolute dielectric permittivity of classical vacuum ($8.859 * 10^{12}$) and ε_r being the dielectric constant of the medium. Consequently, the further the signal is recorded, the less its amplitude.

In addition, it is important to underline that the global effect of several electrical charges is the same as if all the charges were placed in their charge center. This means that all the charges together may be seen as a unique dipole, where the positive charge Q is actually given by the sum of all positive charges (same holds for negative Q).

As a result, for every time instant, it is possible to describe the entire heart activity with a single dipole, which will vary in time, defined as equivalent dipole.

During the depolarization and repolarization processes, the center of all the positive charges doesn't coincide with the center of all the negative charges, hence a dipole vector can be imagined, having the three following characteristics: the amount of electrical charge, the distance between the two opposite charges, and finally the orientation of the line that joins the two charges, i.e. the dipole axis.

Regarding the orientation, it follows that the electrical potential of a dipole in a point P in space, at a distance *d* much greater than the distance *L* between the two charges that form the dipole, is:

$$E(P) = \frac{\mu \cos(\theta)}{4\pi\varepsilon_0\varepsilon_r d^2} \quad (5)$$

where *Q* is the dipole charge, θ is the angle between the dipole axis and the line joining P and the middle point of L, and finally μ is the dipole moment ($Q * L$) (Fig. 18) [14].

As said earlier, it is possible to summarize the electrical activity at a given time in terms of an equivalent dipole, resulting then in a dipole vector.

In particular, the instantaneous axis of the equivalent dipole is referred to as instantaneous electrical axis of the heart. Hence, being the dipole represented by an intensity and a direction, we can define a vector, pointing from positive charge Q to the negative one: what we obtain is the heart vector *H*, which represents the entire electrical activity of the heart at a given time instant. As said earlier, the potential difference varies in time, thus the heart vector varies in time [14]. To detect the electrical activity of the heart, at least two electrodes are required, placed in different positions. Moreover, to have repeatability across different subjects, it is necessary to establish standardized positions for the electrodes.

The Dutch physiologist W. Einthoven proposed to place three limb electrodes at the vertices of an equilateral triangle: one electrode on the right arm (RA), one at the left arm (LA) and the last one at the left leg (LL). In addition, an electrode at the right leg (RL) was introduced simply for noise cancellation purpose, thus not having any diagnostic meaning. To provide faster diagnoses, for instance in an emergency situation or during exercise, Mason-Likar (ML) modified electrocardiogram may be used. In ML-ECG, the RA and LA electrode are actually at the right and left clavicles, whereas the LL and RR electrode are placed on the iliac crests, left and right respectively.

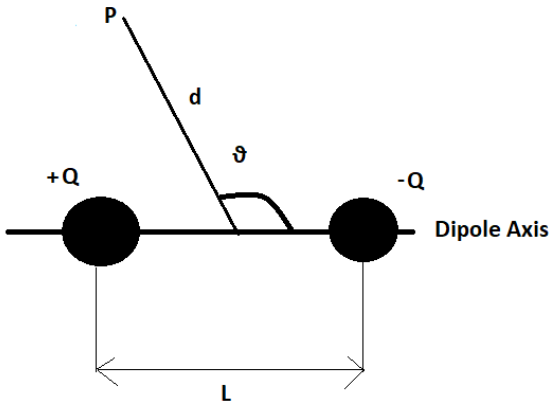

Figure 18. Dipole [14].

Nevertheless, this arrangement doesn't cause significant changes in the signal, since the body is an electrical "volume conductor", and thus the original electrodes positions and ML ones are electrically equivalent. A fourth electrode is placed in the right leg and is used for electrical grounding. This electrode configuration is placed on the frontal plane, hence all the potential differences recorded by the electrodes are the projection of the heart vector *H* on the frontal plane [5].

By considering the equilateral triangle, the straight lines joining RA electrode respectively with LA and LL electrodes, and the line joining the LA electrode with the LL electrode, will define three unit vectors, a_1, a_2 and a_3, respectively defining an axis in the frontal plane at 0, 60 and 120 degrees. Hence, the voltage measured at electrodes RA, LA and LL will be respectively:

$$V_i = H * a_i \tag{6}$$

with i =1,2,3 [5], [14]

In this way, three limb leads are obtained from the Einthoven triangle:

- Lead I, the potential difference between RA and LA, defined as $V_{LA} - V_{RA} = V_1$
- Lead II, that is the potential difference RA and LL, and is computed as $V_{LL} - V_{RA} = V_2$
- Lead III, being the potential difference between LA and LL, and defined as $V_{LL} - V_{LA} = V_3$. [13]

These leads are called bipolar leads, because they do imply two electrodes to read a potential difference [14].

From bipolar leads, unipolar limb leads are obtained.

Unipolar limb leads only measure the potential at a single electrode, with respect to a reference that is obtained as the average of the potentials from the two remaining electrodes.

As a result, three unipolar limb leads can be derived:

- aVR, which measures the potential difference between the RA electrode and the reference got from the LA and LL electrode, and forms an angle of -150 degrees with respect to the frontal plane
- aVL, which detects the potential difference between the LA and the reference at RA and LL, forming an angle of -30 degrees with the frontal plane

- aVF, measuring the potential difference between the LL and the reference from RA and LA, which forms an angle of +90 degrees on the frontal plane.

Since unipolar leads are obtained from the same electrodes used for the bipolar limb leads, this results in unipolar leads representing only the projection of the electrical activity of the heart in the frontal plane (Fig. 19) [5], [14].

Other unipolar leads are derived in the transversal plane, called precordial leads. Six electrodes are placed on the chest, while the reference point is located at the center of the heart, by measuring the average from the three limb electrodes. The reference is called Wilson Central Terminal (WCT). The resulting leads are named V1 to V6. In particular, V1 and V2 are respectively placed on the fourth intercostal space to the right and left of the sternum, whereas V4 is on the fifth intercostal space at the midclavicular line. V3 is positioned halfway between V2 and V4. Finally, V6 is located on the fifth intercostal space at the midaxillary line, while V5 is placed halfway between V4 and V6. (Fig. 20). By including the bipolar leads, the unipolar and the precordial ones, one gets the 12-lead ECG [5], [14].

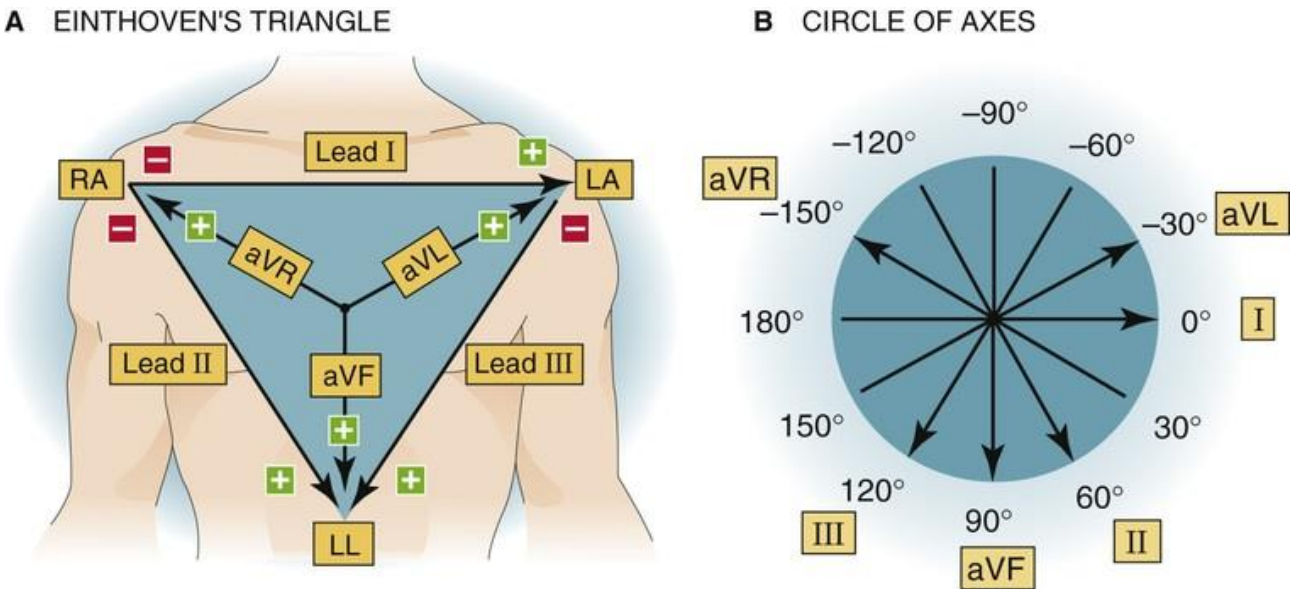

Figure 19. A. Einthoven's triangle. B. Angles of limb leads with respect to the frontal plane [5].

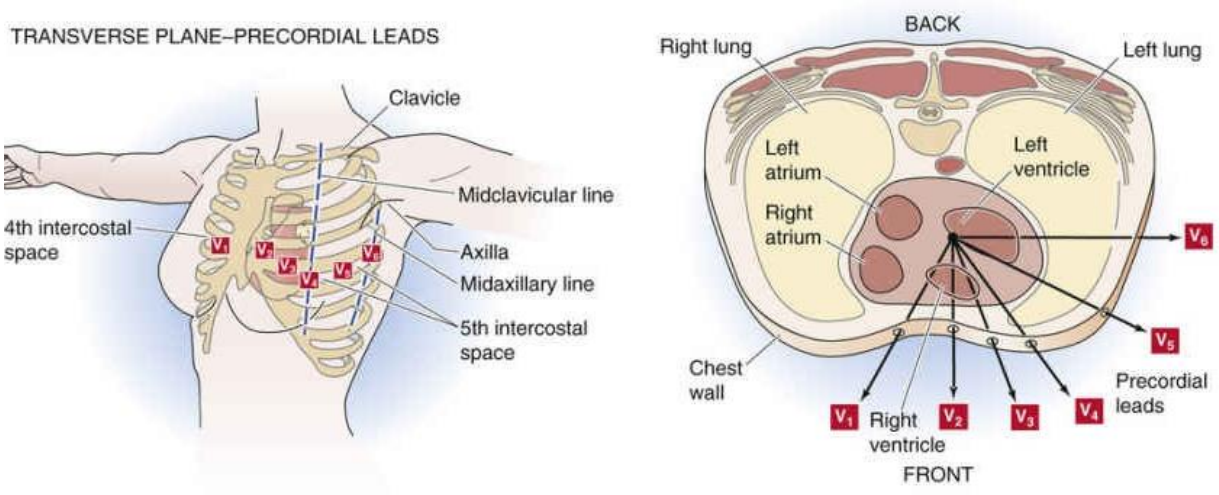

Figure 20. Left: precordial leads displacement on the chest. Right: precordial leads displacement on the transversal plane [5].

The cardiac potential differences are measured with a voltmeter (electrocardiograph), that represents the electrical signal with respect to a reference potential, which is conventionally set to the reference voltage measured in the right leg.

The electrocardiograph is equipped with a galvanometer, which allows to record the oscillations of the electrical signal on graph paper at a standard speed of 25 or 30 $mm \cdot s^{-1}$. Each millimeter on the paper represents 0.04 or 0.02 s, while the standard amplification is 0.1 $mV \cdot mm^{-1}$. For clinical monitoring, the used frequencies are in the range 0.05-50 Hz. However, for diagnostic measurements, the frequency band increases, up to 1 kHz [14].

The output signal of the electrocardiograph is called ECG. It can be considered as a pseudo-periodic signal, and is characterized by fluctuations around the baseline, called waves. The baseline represents the voltage measured by the electrocardiograph when no electrical activity is measured, and it is called isoelectric line.

In most leads, depolarization and repolarization have the same polarity, usually positive. When the depolarization wavefront moves towards a positive electrode, it results in a positive deflection in the voltage, while when moving towards a negative electrode, it appears as a negative deflection. The opposite is true for the repolarization wavefront. As a result, one would expect repolarization and depolarization having opposite polarity, since they travel in the same direction, but have opposite wavefronts. Nevertheless, in most leads, the depolarization and repolarization wavefronts have the same polarity, i.e., the ECG is defined as concordant. The cause is to be found in the different repolarization times of epicardium and endocardium. In fact, the endocardium depolarizes earlier, since the cardiac electrical activity generates in the inner part of the heart. Then,

the depolarization spreads towards the outer layer of the heart, the endocardium. On the other hand, the epicardium has a shorter action potential than the endocardium. Hence, it will repolarize earlier than the endocardium, resulting in a repolarization wavefront moving in the opposite direction with respect to the depolarization. Consequently, depolarization and repolarization will result in the same voltage deflection, which is positive in most leads [5].

The ECG is characterized by segments and waves. Segments are defined as flat portions of the ECG, whereas waves are represented as voltage deflections, and are characterized by minima and/or maxima.

The first wave is called P wave, and represents the depolarization wave that spreads from the SA node throughout the atria. The P wave duration ranges between 0.08-0.1 s. The following waves, called QRS complex, represent the ventricular depolarization; thus, the atrial repolarization is not shown. This happens because the atrial depolarization occurs at the same time as ventricular depolarization and being of smaller amplitude it is hidden by the ventricular activity. After the P wave there is a brief isoelectric period before the QRS complex . This isoelectric part is called PR segment. It goes from the end of the P wave to the beginning of the following wave, and represents the delay of the AV node, i.e., it is the time during which the atria are depolarized and the impulse travels to the AV node, which highly reduces the conduction velocity. The PR segment usually lasts between 0.12 and 0.20 s. After this isoelectric period, the ventricular depolarization starts. This is represented by the QRS complex, lasting between 0.06 and 0.1 s. By comparing this duration with the one of the P wave, it can be noticed that the ventricular depolarization is faster than the atrial one. After the QRS complex, another isoelectric period occurs, called ST segment, since it goes from the end of the QRS complex to the beginning of the following wave, called T wave. During the ST segment, both ventricles are entirely depolarized.

Afterwards, there is the T wave. It represents the ventricular repolarization, and usually lasts longer than depolarization. However, its precise duration is not normally measured.

It is worth mentioning that, after the T wave, sometimes there is the so-called U wave, but researchers still do not agree on its origin.

In addition to segments, it is possible to define intervals, that include wave and segments. For instance, the QT interval goes from the onset of the Q wave to the end of the T wave. This interval has a normal duration between 0.2 and 0.4 s, depending on how fast the heart contracts. The durations of segments, intervals and waves are of extreme importance to identify possible heart problems. For instance, a longer PR than usual, could possibly represent a problem in the

conduction of the impulse in the AV region.
All the intervals, segments and waves that characterize and ECG are shown in Fig. 21, whereas their physiological durations are reported in Table 1 [7].

The HR is defined as the number of cardiac contractions, i.e., beats, per minute. The HR varies according to several factors, including respiration, physical exercise, mental stress etc. Heart Rate Variability (HRV) measures variation in R-R intervals. In fact, the heartbeat is controlled by the autonomic nervous system (ANS), which regulates many body functions and reflects parasympathetic and sympathetic activity [13].
Physiological HR during rest is defined by the American Heart Association (AHA) in the range 60-100 bpm, even though some suggest lowering the upper limit to 85 bpm [15].

Three main types of ECG tests exist:

1. Resting ECG: it is carried out while the patient is at rest, lying on his back. The test usually lasts between one and five minutes.
2. Exercise ECG: during the test, the patient does physical exercise; he usually rides an exercise bike. The patient steadily increases the level of the physical activity. This test also provides the power generated in Watts through the bike.
3. Holter monitor: the test usually lasts 24 hours. The electrodes, placed on the skin of the patient, are connected to a small recording device, worn by the patient himself on a belt or hung around the neck. When the test finishes, the data are downloaded on a computer by the doctor, who then analyzes the ECG. Moreover, in order to have a better interpretation of the signal, the patient is asked to write all the activities he performs while undergoing the test. This test is usually used when the two previously described test do not show clear results about the health of the patient [16].

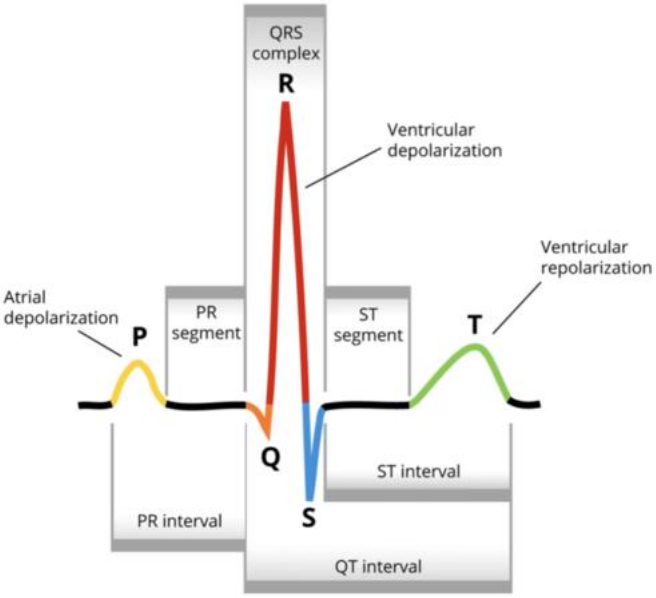

Figure 21. The ECG

Table 1 – Duration of ECG components [7].

ECG COMPONENT	NORMAL DURATION (s)
P wave	0.08-0.10
QRS complex	0.06-0.10
T wave	Not normally measured
PR interval	0.12-0.20
ST segment	Not normally measured
QT interval	0.20-0.40

3 EXTRACTION OF THE RESPIRATORY SIGNAL FROM THE ELECTROCARDIOGRAPHIC SIGNAL

3.1 RESPIRATORY MODULATION OF THE ELECTROCARDIOGRAPHIC SIGNAL

The respiration has some effect on the ECG, that is saying the ECG is influenced by the respiration. Three respiratory modulations can be noticed: baseline wander (BW), amplitude modulation (AM), and frequency modulation (FM) (Fig. 22).
Changes in the orientation of the heart's electrical axis with respect to the electrodes, and changes in thoracic impedance cause BW and AM. Indeed, heart displacements lead to the motion of the electrodes relative to the heart, which in turn cause a rotation of the electrical axis of the heart [17].

Being the pericardium fused to the diaphragm, diaphragmatic movements result in heart displacements. During inspiration, the downward movement of the diaphragm pulls the heart in a more vertical position, and makes it descend. In this way, both the QRS axis and the T wave axis shift to the right. On the other hand, during expiration, the diaphragm relaxes and elevates, hence the apex of the heart will be compressed toward the breast, shifting the QRS axis back to the initial position, previous to inspiration [17], [18], [19].
By considering, for instance, the QRS complex, it can be noticed that, as a result of heart displacements, during inspiration the QRS amplitude decreases and increases with expiration. Certainly, deep respiration amplifies the effects on QRS amplitude. On the other hand, during apnea events, the QRS axis has been demonstrated to shift towards the left and being associated with a decrease in its maximum [20], [21], [22].

Differently, FM is the manifestation of the spontaneous changes in HR during respiration, known as respiratory sinus arrhythmia (RSA). During inspiration, the HR increases, while it decreases during expiration. RSA is caused by several mechanisms. The most important are, as follows:

- changes in intrathoracic pressure during inspiration stretch the SA node, resulting in shorter RR intervals, and thus faster HR;
- increased vagal outflow during expiration, which reduces HR;

- reduced intrathoracic pressure during inspiration decreases left ventricular stroke volume, which results in a baroreflex mediated increase in HR.

It must be underlined that, some modulations of the ECG can vary, for instance, with age. In fact, FM is highly reduced in elderly subjects [18].

By exploiting the respiratory modulation on the ECG, it is possible to extract the RS from the ECG, generating the EDR signal. This extraction is considered to be a very powerful tool, since it enables to derive a continuous RS, hence relative to the respiratory system, from another signal which describes the physiology of another system, i.e., the cardiovascular one. As a consequence, this method results in a very convenient procedure, since by only measuring ECG, one can surely analyze cardiac activity, but also retrieve information on the RS. EDR measurements can be applied for instance when trying to avoid a too much laborious instrumentation set, including for instance wearable sensors. Especially, EDR is highly suitable in those patients where direct RS measurements cannot be performed. In fact, in this way, the RS can be monitored indirectly.

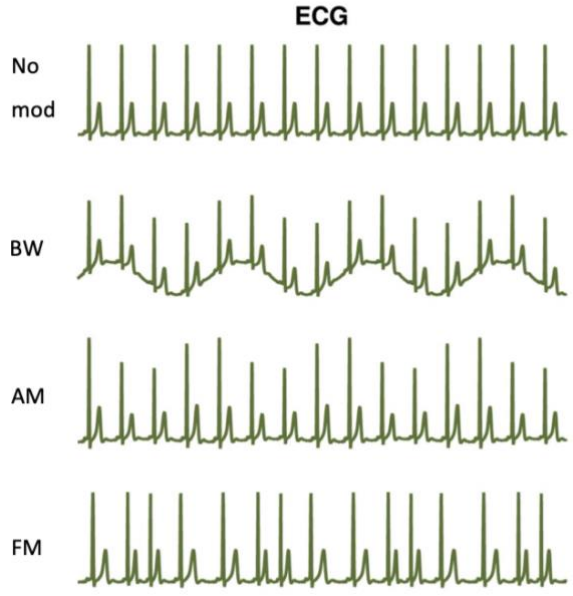

Figure 22. No modulated (No mod) ECG compared with modulates ECGs, respectively baseline wander (BW), amplitude modulation (AM) and frequency modulation (FM) [18].

3.2 CURRENT STATE OF THE ART

Over the years, several techniques have been proposed in the literature, in order to extract EDR signal. These techniques exploit the respiratory modulation that affects the ECG.

3.2.1 Elimination of the very low frequencies

The first thing to do when extracting respiration from the ECG is the elimination of the very low frequency (VLF) components, i.e., those at sub-respiratory frequencies. This is usually carried out through high-pass (HP) filtering with cut-off frequencies ranging between 0.03 and 0.05 Hz. Typical HP filtering techniques include median filter, subtraction of a baseline trend by using a linear polynomial fit, or baseline measurements at points in the cardiac cycle [18].

3.2.2 Extraction of respiration

After the pre-processing, several methods can be applied to extract EDR, including filter-based techniques and feature-based techniques [18].

***3.2.2.1** Filter-based techniques*

Filter-Based Techniques extract EDR by filtering the ECG. In particular, the ECG is filtered in a way that non-respiratory frequency components are attenuated.

3.2.2.1.1 Wavelet analysis derived respiration

Wavelet analysis generates a time-scale representation of a one-dimensional signal. Its frequency localization is logarithmic, hence time localization gest finer in the highest frequencies. The Wavelet Transform (WT) is defined as the sum over time of a signal multiplied by the scaled and shifted version of a wavelet function ψ. The WT of a signal *x(t)* is defined as in (7), with *a* and *b* being respectively scaling and shifting coefficients:

$$W_a x(t) = \frac{1}{\sqrt{a}} \int_{-\infty}^{+\infty} x(t)\ \psi\left(t - b/\sqrt{a}\right) dt,\ a > 0 \qquad (7)$$

Wavelet decomposition works by decomposing a signal, at each decomposition level, into two components, respectively an approximation and a detail coefficient. The approximation coefficient captures LF components, whereas the detail coefficient captures high-frequency (HF) components. When applying DWT, a mother wavelet must be chosen. The choice is usually made by selecting a mother wavelet that is as similar as possible to the analyzed signal. Afterwards, the level of decomposition *N* is chosen, depending on needs. (Fig. 23). In particular, the DWT can be used to extract the RS from the ECG by selecting a frequency interval on an appropriate level of decomposition.

Labate et al. [23] have proposed EDR extraction by means of Discrete Wavelet Analysis (DWT), by using Mallat fast algorithm. [23] [24] They chose a 9^{th} order level decomposition and used four different mother wavelets: Daubechies of 3^{rd} (db3) and 6^{th} order (db6) and Symlet of 3^{rd} (sym3) and 6^{th} (sym6) order. The RS was reconstructed by taking the detail signal of the 9^{th} decomposition. The most suitable mother wavelet for EDR extraction resulted to be Daubechies of 6^{th} order, having the highest coherence with the synthetic RS signal they used as a reference (Fig. 24). By looking at Table 2, it can be noticed that DWT well resembled the respiratory frequency of the reference RS, however it did not allow a unique reconstruction of the respiratory waveform, as shown in Fig. 25. The main drawback of DWT is that its energy distribution in the time domain depends on the coherence between the signal and the selected mother wavelet. In fact, if a signal is not coherent with the frame, as it usually happens for noise components, then the energy is spread over many coefficients having low magnitude.

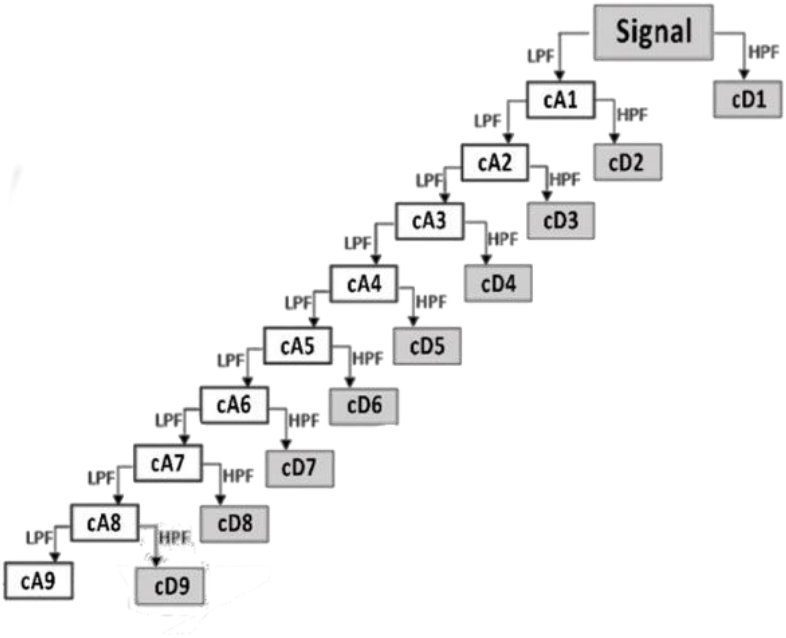

Figure 23. Wavelet decomposition on 9 levels

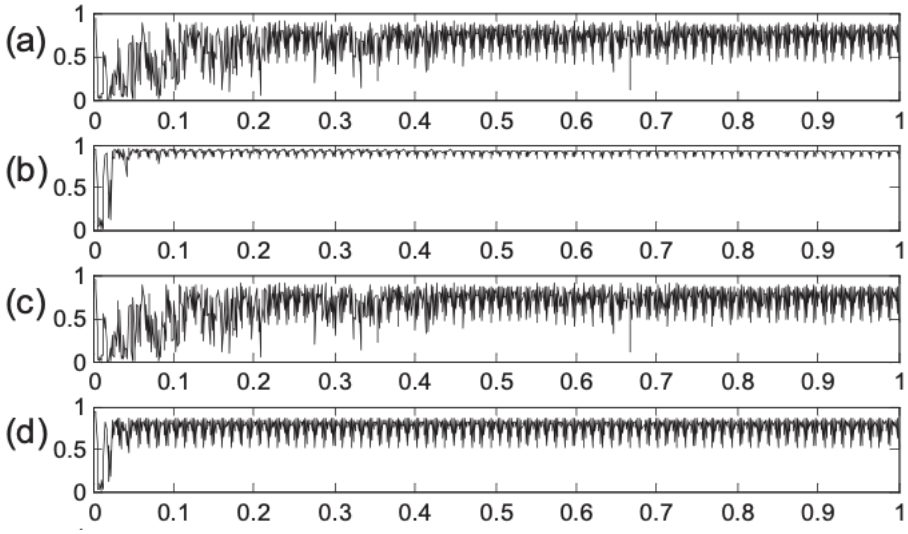

Figure 24. Comparison of coherence between the extracted RSs and the synthetic RS. [a] db3. [6] db6. [c] sym3. [d] sym6 [23].

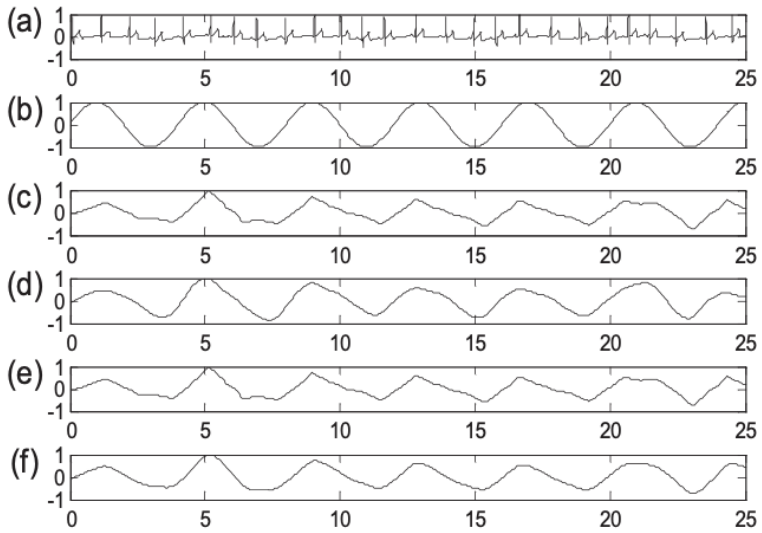

Figure 25. Comparison between synthetic RS and EDR extracted by applying DWT. a). Real ECG modulated by synthetic RS, b) synthetic RS, c) EDR by WT with db3, d) db4, e) sym3, f) sym6 [23].

Table 2. Frequency occurrence, frequency centroid (Δf) and correlation coefficient [23].

	Frequency (Hz)	Δf	Correlation
Synthetic RS	0.25	0	100%
Wavelet: db3	0.26	0.07	89.34%
Wavelet: db6	0.26	0.04	92.14%
Wavelet: sym3	0.26	0.07	89.34%
Wavelet: sym6	0.26	0.03	93.01%

3.2.2.1.2 Empirical mode decomposition derived respiration

Empirical Mode Decomposition (EMD) can be used to derive RS as well. In fact, EMD separates time-series into intrinsic oscillations using local temporal and structural characteristics of the data. EMD is actually achieved through a linear sum of components that approximate the original ECG signal [25].

EMD starts by estimating a signal as a sum of a local trend and a local detail, being respectively a LF part and a high frequency (HF) part. The detail is referred to as Intrinsic Mode Function (IMF) while the local trend is called residual. After this estimation, the procedure is applied again to the residual, considered as a new time-series, in a way that a new IMF and a new residual are obtained. This process is then iterated. In the end, the reconstructed signal will be defined as the sum of a finite

number of IMFs and a final residual. By considering a signal *x(t)* the EMD algorithm can be described as it follows and is represented in (Fig. 26):

1. Identification of maxima and minima of *x(t)*
2. Generate the upper and lower envelope by connecting the maxima and minima points separately with cubic spline
3. Compute the local mean *r(t)*, as half the sum of the envelopes
4. Extract the detail *d(t) = x(t) – r(t)*
5. Iterate on the residual *r(t)*

When the decomposition process ends, the EMD method expresses the signal *x(t)* as the sum of a finite number of IMFs and a final residual, as described in (8)

$$x(t) = \sum_{i=1}^{n} h_i(t) + r_n(t) \quad (8)$$

Although EMD have some common features with WT, one big difference must be highlighted. In fact, unlike WT, EMD decomposition basis is not fixed a priori, but uses adaptive bases that are directly generated from data [26].

[23] derived EDR by using EMD, by a visual inspection and following selection of IMFs related to the respiratory activity. The obtained EDR highly resembled the frequency spectrum of the reference synthetic RS signal, as shown in Table 3. Moreover, as shown in Fig. 27, the RS waveform showed high similarity with the one from the reference synthetic signal. Beyond the good results of EMD, the authors highlighted a major limitation of EMD, being its empirical grounding, hence lacking theoretical basis.

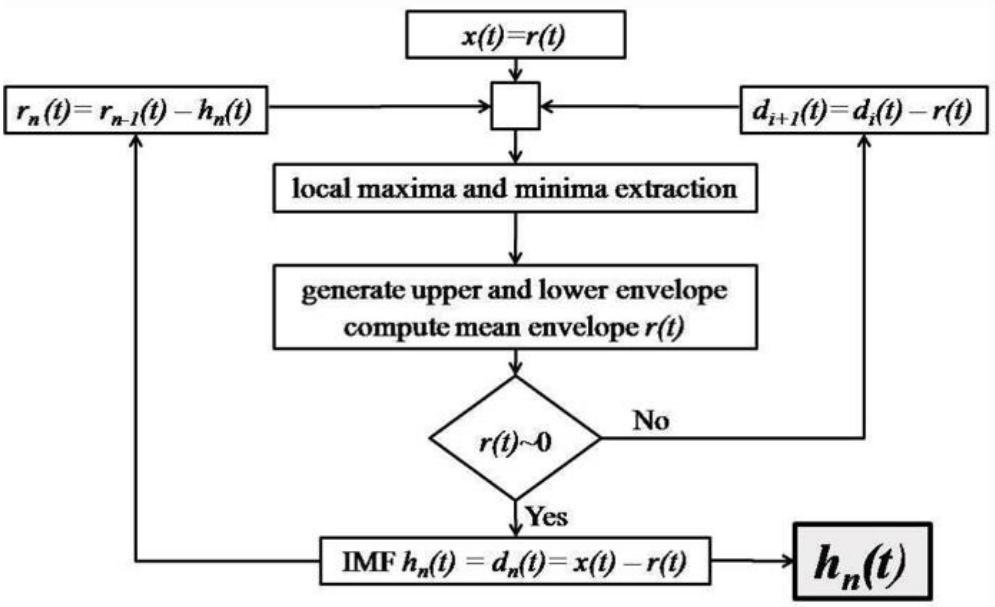

Figure 26.. Block Diagram of the IMF extraction in EMD [23].

Table 3. Frequency occurrence, frequency centroid (Δf) and correlation coefficient [23].

	Frequency (Hz)	Δf	Correlation
Synthetic RS	0.25	0	100%
EMD	0.26	0.01	93.07%

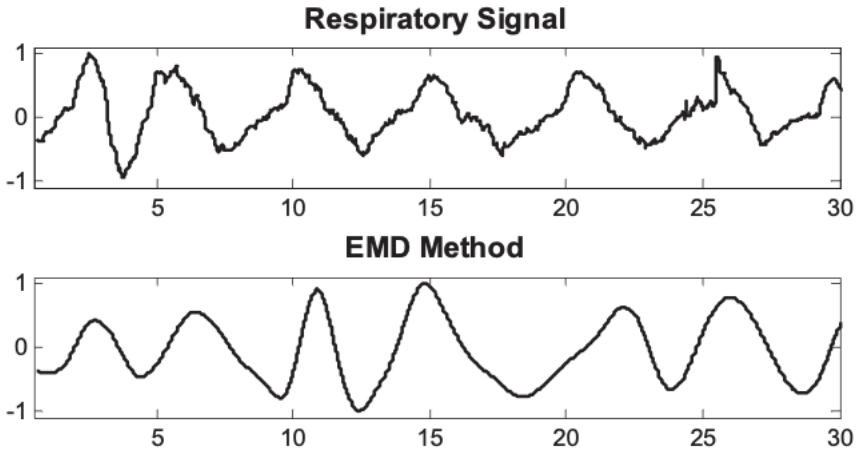

Figure 27. Synthetic RS and EDR extracted by EMD [23].

3.2.2.1.3 Electromyogram derived respiration

In 1913 W. Einthoven noticed for the first time periodic bursts of HF muscle noise in some 12-lead ECGs. [27] The ECG contains muscle tremor noise from electrical activation of inter-costal chest muscles and the diaphragm during the respiratory cycle. Thus, by specifically filtering the ECG, the electromyogram (EMG) can be found and can be used to extract the RS. [28] filtered the ECG with a HP filter at 250 Hz, since they found the EMG to have a center frequency between 250 and 500 Hz. To identify the power of the muscle activity, the root mean square (RMS) of the signal was computed in a 51 ms sliding window. Since after the previous filtration, the QRS still remained as spikes, the following step consisted in running a QRS detector in order to eliminate the spikes. Finally, a simple moving average (SMA) filter was applied to low pass smooth the RMS signal into the final EMG-DR (Fig. 28). However, this technique strongly relies on patient's movement, since also small movements can be detected in EMG and can thus corrupt the EMG-EDR signal [28].

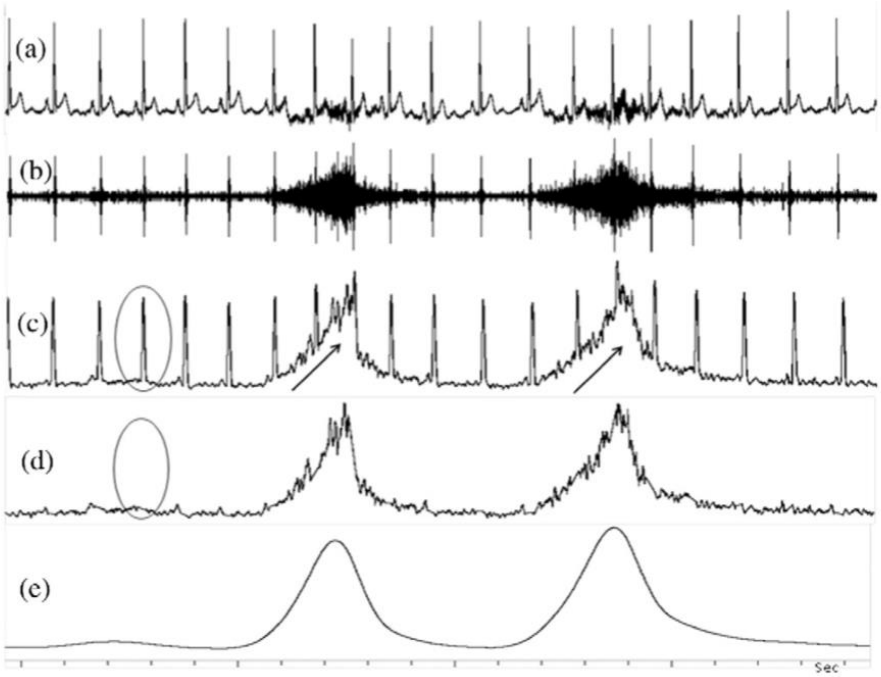

Figure 28. a) Raw ECG. b) 250 Hz filtered ECG. c) RMS computation. d) QRS detection and elimination. e) final EMG-DR signal [28].

3.2.2.2 Feature-based techniques

Feature-Based Techniques extract beat-by-beat feature measurements [18].
EDR algorithms can be based on beat morphology or on HR information, but there also some which are based on both [21].

3.2.2.2.1 Amplitude modulation derived respiration

Khaled et al. [29] have proposed to extract respiration by exploiting the AM of the ECG, specifically by exploiting the modulation on the R wave, realizing a method called Cardio-Modulo-Respirography (CMR).
In order to remove muscular and movement artifacts, together with the baseline noises, the ECG was first passband filtered (2.5-25 Hz). Later, a peak detector is used, which controls a Sample and Hold circuit for each maximal R wave. Then the RS is obtained (Fig. 29). They compared their results with a classical method of Impedance Rheography (IR).
CMR resulted to be insensitive to both cardiac and movements artefacts, and thus proved to be a valid method. Fig. 30 shows the CMR and IR from an infant. It can be clearly seen that while IR was affected by cardiac artefacts during a central apnea, CMR resulted in being insensitive to such artefacts. In addition, Fig. 31 shows that CMR did not detect movement artefacts during apnea, unlike IR. The only drawback of CMR regards the verification of Shannon's law for sampling frequency, since the cardiac frequency must be at least twice as big as the respiratory frequency to obtain a real representative RS.

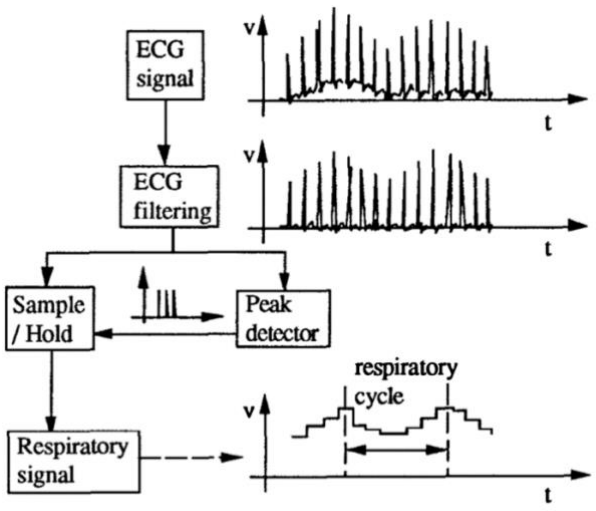

Figure 29. System Block diagram of CMR [29].

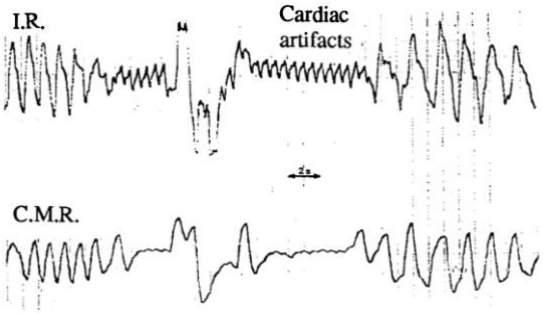

Figure 30. CMR and IR from an infant [29].

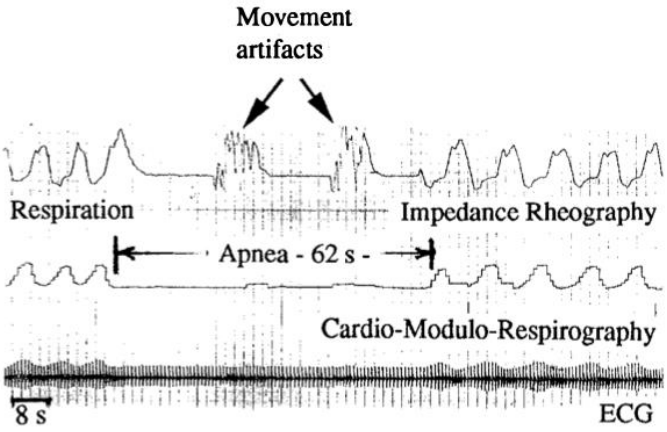

Figure 31. Recordings from a 28 years old adult [29].

3.2.2.2.2 Cardiac axis deviation derived respiration

Another method to extract EDR is by analyzing cardiac axis deviation during respiration, since this induces an apparent modulation in the direction of the mean cardiac electrical axis [21]. Moody et al. [30] studied the deviation of the QRS complex, by exploiting two ECG leads. In particular, after having subtracted the baseline, the authors measured the area of each normal QRS complex over a fixed window width. In this way, the QRS area is proportional to the mean amplitude of the signal, therefore it is also proportional to the projection of the mean cardiac electrical vector on the lead axis. Assuming that the leads are orthogonal, measuring the arctangent of the ratio of the areas from the two leads gives the angles of the mean axis with respect to the lead axis (Fig. 32). If the two leads are not orthogonal, some errors may be present. By measuring axis direction during the QRS complex, one sample of EDR per cardiac cycle is obtained. Then by interpolation using cubic splines, a continuous EDR signal is produced. To obtain additional samples, the mean axis direction during the T wave can be measured. The authors also ensured that this method may be applied when using a single ECG lead, even though in this case the single lead EDR works best if the lead axis is significantly different from the mean electrical axis [30].

To evaluate their results, [30] simultaneous recordings of ECG (with two orthogonal leads) and pneumatic respiration transducer (PRT) were carried out. Their results showed strong correlation with conventional measurements of respiration (Fig. 33). Nevertheless, respiratory disturbances which are reflected only in TV changes, may not always be detected using this method.

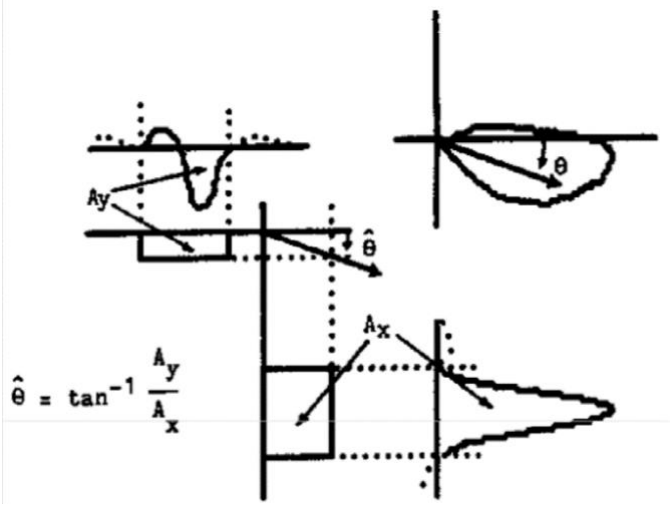

Figure 32. Estimation of cardiac axis direction from QRS area measurements [30].

Figure 33. Central apnea. Upper trace: EDR. Lower trace: chest PRT [30].

Helfebein et al. [28] have tried to simplify the work of Moody by measuring the total QRS amplitude in a single lead, instead of measuring the QRS area in two leads. First, they identified the beats with a QRS detector, then measured the total QRS amplitude. Afterwards, they removed outlying values greater than two standard deviations from the running mean (e.g, artefact) and later reconstructed the RS by using the QRS amplitude as the respiration signal amplitude at each beat. In the end, cubic spline interpolation was used to reconstruct a continuous EDR, which was then filtered according to the performed respiration (Fig. 34).

Even though this method showed to be relatively resistant to muscle artifact, a major drawback is that it may miss apnea episode if QRS axis shift occur but without airflow. Moreover, another disadvantage is that EDR phase may not correspond with peak TV [28].

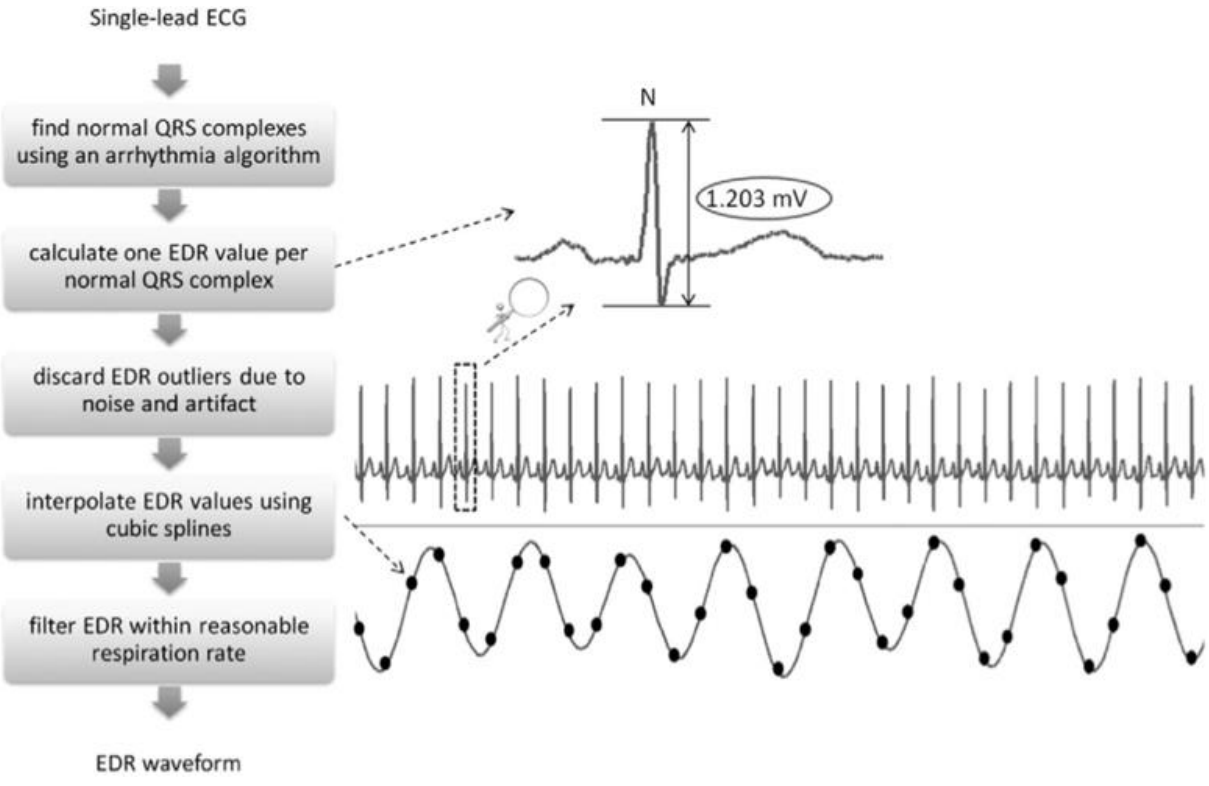

Figure 34. EDR extraction from single-lead ECG [28].

3.2.2.2.3 Heart rate variability derived respiration

Campolo et al. [26] proposed a method to extract EDR by exploiting RSA, hence HRV. In fact, as said earlier, instantaneous HR (IHR) varies with respiration, increasing during inspiration and decreasing with expiration. The authors obtained EDR by means of interpolation of the amplitude values of the R peaks. In order to remove noise from the signal, the authors first applied a 20^{th} order filter, high pass FIR filter, which has as cut-off frequency of 0.05 Hz. Then a notch filter was used to remove the frequency component at 50 Hz. The R-peaks were detected by using Pan-Tompkins detector algorithm. Later, the maximal value of the filtered ECG signal in a 20 ms window around the QRS peak is taken and the time index is noted. With this process, two discrete-indexed vectors are produced, where one contains the R peak amplitudes, while the other includes the R peak occurrence. Afterwards, a discrete-time sequence is generated and initialized with all zero values. This sequence is then filled with the R peak amplitudes at the sample near to the R peak occurrence times. Finally, the new obtained signal is filtered with a 5^{th} order, low pass, Butterworth filter, at a cut-off frequency of 0.04 Hz, leading to a smooth EDR signal. The authors evaluated the method in three conditions, being respectively supine, standing and light activity. Table 4 reports the results. It can be clearly seen that the method bets performed in supine state, but the results were generally not very good.

Helfebein et al. [28] have also proposed a method for EDR extraction that exploits RSA. In this study, the authors used each QRS complex R-R interval in the ECG to obtain the IHR, defined as the inverse of R-R, and then used it as the amplitude for the respiration signal. Then, by means of cubic spline interpolation, the final respiratory waveform has been produced (Fig. 35). One big advantage of this method is that only QRS locations need to be defined, and their detection is fairly resistant to muscle artifact. Results showed the proposed method well resembles the original RS. However, the main disadvantage of RSA is its limited application. In fact, RSA naturally decreases with age or illness, making it difficult to define a unique method for all ages. Moreover, since the respiratory wave samples are only extractable at QRS times, the RS may be under sampled, beyond being strongly dependent on the accuracy of the cubic spline [28].

Table 4. Correlation coefficient (C) between recorded and ECG-derived RS. Evaluation accuracy (A) of the respiratory frequency [26].

	HRV method	
	C	A (%)
Supine	0.10	87%
Standing	0.07	85%
Light activity	0.04	75%

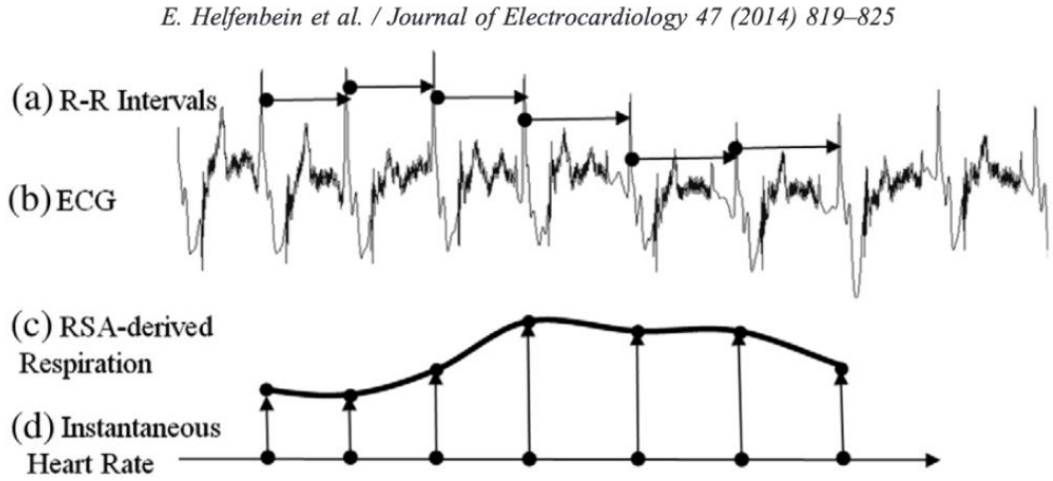

Figure 35. RSA- derived respiration. Horizontal arrows (a) represent R-R intervals in the ECG (b). The inverse of R-R intervals (c) represented with vertical lines, are used to construct the RS (c) by using cubic spline interpolation [28].

3.2.2.2.4 QRS slope and R wave angle derived respiration

Another method to obtain EDR consists in measuring the QRS slope and the R wave angle. Lazaro et al. [31] evaluated this method over two databases, respectively during a tilt test and a stress test. The QRS slope were measured by using the algorithm presented in Pueyo et al. [32] Two slopes are measured for each beat, respectively the upward (U_R) and downward (D_R) slopes of the R wave. The time instants associated with the maximum variation points of the ECG between the Q (n_Q) and R (n_R) peaks, and between R (n_R) and S (n_S) peaks are computed as in (9) and (10)

$$nU_R = \max\{|\, l_l'(n)|\} \qquad n \in [nQ, nR] \tag{9}$$

$$nD_R = \max\{|\, l_l'(n)|\} \qquad n \in [nR, nS] \tag{10}$$

where $l_l'(n)$ is the first derivative of lead l:

$$l_l'(n) = l_l(n) - l_l(n-1) \tag{11}$$

In the end, a straight line is fitted to the ECG signal for $nU_R$and another for nD_R. The slopes are then defined as I_{UR} and I_{DR}.

Regarding the R wave angle, it corresponds to the smallest one formed by the two straight lines just mentioned, so that assuming a 2D Euclidean space coordinate system, the angle becomes:

$$\phi = \arctan\left(\frac{|\mathrm{I}_{UR} - \mathrm{I}_{DR}|}{|1 + \mathrm{I}_{UR}\mathrm{I}_{UR}|}\right) \tag{12}$$

EDR signal was then generated starting from QRS slopes by taking the value of the slopes at each QRS occurrence n_N, as in (13)

$$d_{(UR,DR)}(n) = \sum_i I_{(UR,DR)}\delta(n - n_N) \tag{13}$$

In a similar way, the EDR was obtained from the R wave angle as in (14)

$$d_R(n) = \sum_i \phi_R\delta(n - n_N) \tag{14}$$

The final EDR signal was obtained by combining EDR signals from all 12 leads. Afterwards, the authors applied an algorithm to extract the BB interval and found low estimation errors compared to a RS used as the reference, hence demonstrating the goodness of this technique. However, the authors themselves stressed out that using all 12 leads to extract EDR may result unmanageable in some situations, such as ambulatory scenarios.

3.2.2.2.5 Phase-Space reconstruction derived respiration

Further techniques to extract EDR regard the phase-space reconstruction of single ECG lead, which covers temporal characteristics, as shown by [33]. [33] used lead II. They dataset they used included people performing a series of static physical activities, stand, supine, left-lateral lying, and right-lateral lying. First, QRS detection was performed and verified, including only normal heartbeats. The authors employed the major portrait radius (MPR) that is derived from the phase space of the ECG.

The phase space reconstruction expands a time series *x(t)*, with *t = 0…T*, into a series of vectors **x**(t), *t = 0…T-(d_m-1)*τ as in (15)

$$\boldsymbol{x}(t) = [x(t) \;\; x(t+\tau) \;\; \ldots \;\; x(t+(d_m-1)\tau] \tag{15}$$

where τ is a constant time delay and d_m is the embedding dimension. By putting vector **x**(t) in multiple dimensions, the phase space trajectory of the time series can be visualized. The authors used a two-dimensional phase space diagram (d_m = 2) to reconstruct the phase space of the QRS complex and set τ at 8 ms. To better compare their results, [33] also computed EDR by using two assessed EDR extraction methods, being the AM and the HRV derived respirations. Fig. 36 reports the coherence between the obtained EDR and the reference RS. It can be appreciated that MPR-based EDR gave the best results. The coherence quantified temporal relationships. Nevertheless, frequency relationships must be investigated too, to better assess the goodness of this method.

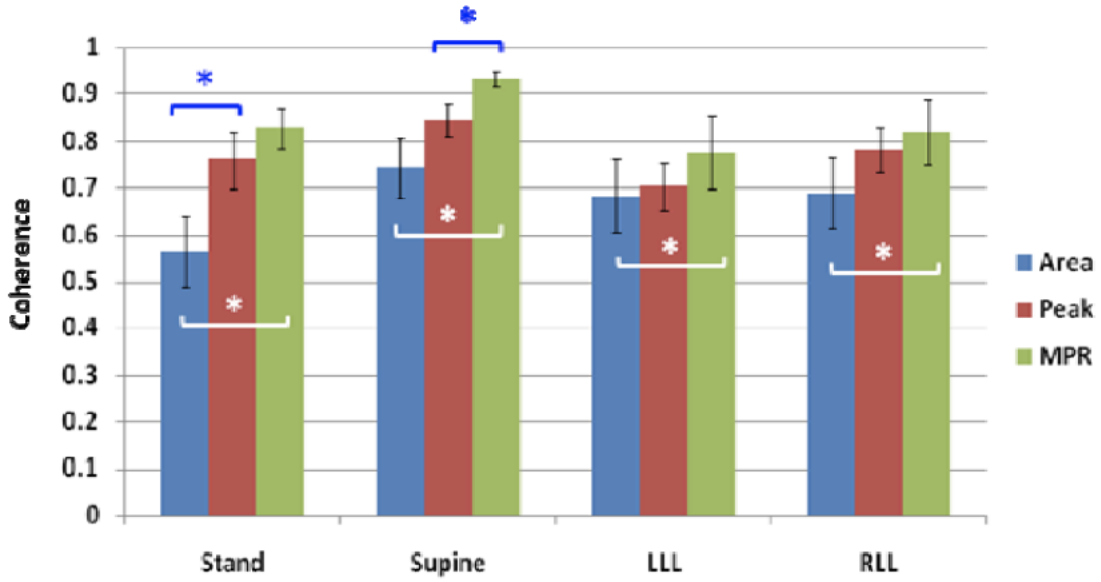

*Figure 36. Coherence between EDR and the reference RS. * indicating significant difference [p<0.05] [33].*

3.2.2.2.6 Iterated Hilbert transform derived respiration

The Hilbert transform (HT) of a signal g(t) is the convolution of g(t) with the signal $1/\pi t$. It is the response to g(t) of a linear time-invariant filter having impulse response of $1/\pi t$.

$$\mathcal{H}[g(t)] = g(t) * \frac{1}{\pi t} = \frac{1}{\pi} \int_{-\infty}^{+\infty} \frac{g(\tau)}{t-\tau} d\tau \quad (16)$$

Recently, the iterated HT (IHT) has been proposed for multi-component AM-FM signal analysis, for non-stationary signals. Since the QRS complexes in the ECG are modulated during respiration, these variations in the waveform can be reconstructed as EDR signal by using the IHT, as proposed by Sharma et al. [34] The authors used a dataset including healthy people in a resting state. Considering an ECG signal *x(t)*, the multi-component AM-FM model by using the IHT becomes:

$$x(t) \approx \sum_{j=0}^{N} \frac{\bar{a}_j(t)}{2^J} \sum_{i=1}^{2j} \cos[\Phi_j^i(t)] \quad (17)$$

where $\bar{a}_j(t)$ and Φ_j^i respectively represent the amplitude envelope and phase in the jth iteration of the multicomponent AM-FM decomposition, while N represent the total number of ECG components. The amplitude envelopes computed in the initial iteration of the decomposition carry the low-frequency information of the decomposed signal, and since the RS is a LF one, it can be exactly derived from the $\bar{a}_j(t)$ components. To extract EDR, it is first needed to remove the unwanted frequency components from the amplitude components $\bar{a}_j(t)$. The authors eliminated the unwanted frequencies by employing a 10th order Butterworth pass band filter, between 0.1 and 0.5 Hz. Later, in order to only select the components that best represent the RS, [34] computed the ratio P_J, defined as the ratio between the power in the respiratory frequency band and in the total band of $\bar{a}_j(t)$ component. The component with the highest ratio was selected as EDR signal. To assess their method, [34] also used two well-known methods, being respectively the HRV and the AM derived respiration methods. Fig. 37 represents the correlation between the recorded RS, taken as reference, and EDR from the three mentioned methods. It can be noticed that IHT method had the highest correlation. However, this study only dealt with controlled situations in health people, hence no application of this new method has been tested on noisy data and patients having either cardiac or respiration problems.

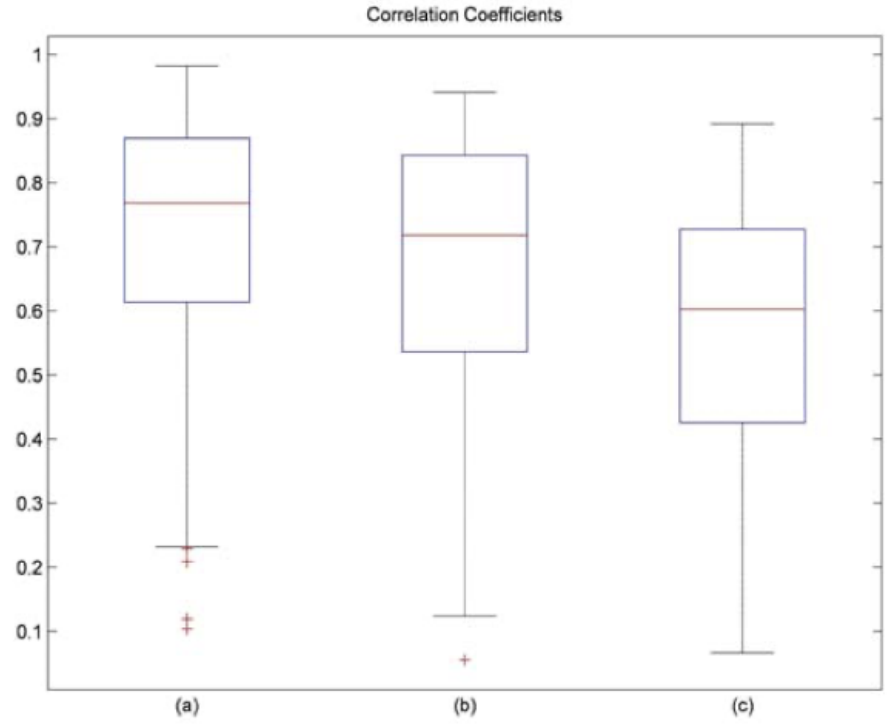

Figure 37. Boxplot representation of correlation computed between the reference RS and the derived respiration methods using a) IHT, b) AM, c) HRV [34].

4 DATA COLLECTION AND STRUCTURE

4.1 CLINICAL DATA

Data were collected at the Cardiovascular Bioengineering Laboratory at Università Politecnica delle Marche (Ancona, Italy), from 2019 to 2022 and organized in a database, called 'Respiration Database', for a total of 50 subjects. All subjects were supposed healthy, had no cardiac disease, at the acquisition time. Table 5 and 6 contain clinical data of all subjects, including sex (‘M’ = male or ‘F’ = female), age (years), height (cm), weight (kg), smoking attitudes (‘YES’ = smoker, ‘NO’ = no smoker, ‘EX’ = ex-smoker), sport history (‘YES’ = athlete, ‘NO’ = non-athlete, ‘EX’ = ex-athlete) and COVID-19 history (‘YES’ = the subject had tested positive to COVID-19 virus in the past, ‘NO’ = never tested positive to COVID-19 virus).

Table 5. Clinical data from Respiration Database for female subjects.

Subject	Sex M/F	Age (years)	Height (cm)	Weight (kg)	Smoker YES/NO/EX	Athlete YES/NO/EX	COVID-19 YES/NO
1	F	23	163	63	NO	NO	YES
2	F	24	159	58	NO	SI	NO
3	F	21	175	70	NO	NO	NO
4	F	19	158	50	NO	YES	NO
5	F	23	160	60	YES	NO	YES
6	F	23	174	68	NO	NO	YES
7	F	22	170	52	NO	NO	YES
8	F	23	169	52	NO	NO	NO
9	F	22	161	56	EX	NO	YES
10	F	22	165	53	NO	EX	NO
11	F	23	170	58	NO	NO	NO
12	F	20	160	53	YES	YES	NO
13	F	22	151	54	NO	NO	YES
14	F	21	171	71	NO	NO	NO
15	F	21	160	60	NO	EX	YES
16	F	21	164	54	NO	NO	NO
17	F	21	160	64	YES	YES	NO
18	F	21	160	60	YES	NO	YES
19	F	23	163	56	NO	EX	NO
20	F	23	166	65	NO	EX	YES
21	F	25	176	67	YES	YES	NO
22	F	20	167	58	NO	NO	NO
23	F	22	151	48	NO	NO	NO
24	F	21	160	54	NO	NO	NO
25	F	21	175	63	NO	NO	NO
26	F	25	158	49	NO	NO	NO
27	F	21	155	50	NO	NO	NO

Table 6. Clinical data from Respiration Database for male subjects.

Subject	Sex M/F	Age (years)	Height (cm)	Weight (kg)	Smoker YES/NO/EX	Athlete YES/NO/EX	COVID-19 YES/NO
28	M	26	185	70	NO	NO	NO
29	M	25	169	66	EX	NO	YES
30	M	25	175	70	NO	YES	YES
31	M	21	178	74	NO	YES	YES
32	M	21	171	62	YES	NO	NO
33	M	26	183	80	NO	EX	NO
34	M	23	173	73	NO	YES	NO
35	M	23	180	68	NO	NO	NO
36	M	24	180	65	NO	NO	YES
37	M	21	180	83	NO	YES	YES
38	M	23	180	88	YES	YES	YES
39	M	21	178	89	NO	YES	YES
40	M	22	184	75	NO	YES	YES
41	M	23	180	74	NO	YES	YES
42	M	21	178	84	NO	EX	YES
43	M	22	183	77	YES	NO	NO
44	M	26	180	78	YES	EX	YES
45	M	23	170	68	NO	EX	NO
46	M	21	184	72	NO	NO	NO
47	M	21	172	67	NO	NO	NO
48	M	54	178	68	NO	NO	NO
49	M	24	183	72	NO	NO	YES
50	M	32	179	77	YES	YES	NO

4.2 DATA ACQUISITION

4.2.1 Acquisition instrumentation

All subjects underwent a 12-lead ECG recording, by wearing the Holter device M12R HOLTER & ECG RECORDER by Global Instrumentation (Fig. 38). This device can be configured to record continuous ECG (Holter Mode), to record intermittent real-time recording (ECG capture) or to run both simultaneously. It can be configured to acquire either 3-channel or 12-lead ECG by changing the patient cable. The device employs either a sampling frequency of 1000 Hz or 250 Hz, according to the user's need, with a resolution of 0.5 mV. The M12R uses low-cost standard SD data storage cards that are easily removable to enable immediate recorder use [35].

In addition to the Holter device, during the test some subjects also wore a chest strap, specifically the BioHarness 3.0 by Zephyr. The chest strap provided a reference signal for respiration, determining the BB interval, beyond measuring many other parameters, including ECG and HR. The device is made of a conductive belt, through which signals are acquired, and a small electronic module (Fig. 39) [36].

Figure 38. M12R HOLTER & ECG RECORDER by Global Instrumentation [35].

Figure 39. BioHarness 3.0 by Zephyr [36].

4.2.2 Acquisition protocol

Before the acquisition started, the subject was asked to remove any metallic objects and to lie bare chest on the bed. Excessive chest hair was removed to better apply electrodes. The SD data storage card was initialized with subject data, and the sampling frequency was set at 1000 Hz. Afterwards, electrodes were applied following M-L configuration in order to get a 12-lead ECG. Electrodes were positioned in the following order, as represented in Fig. 40:

- RA and LA electrodes were respectively placed 2 cm below the third external distal of right and left clavicle;
- V1: on the 4th intercostal space on the right sternal edge;
- V2: on the 4th intercostal space on the left sternal edge;
- V6: on the median point of the left axillary line;
- V5: on the left anterior axillary line;
- V4: on the 5th intercostal space on the median point of the left clavicular line on the same horizontal axis as V5;
- V3: halfway between V2 and V4;
- RL and LL were placed halfway between the ribs and the right, or left, respectively, ileum.

After the electrodes had been placed, some subjects also wore the chest strap BioHarness 3.0 by Zephyr, which was fastened around the abdomen of the subject. The protocol included two stages, for a total duration of around 20 minutes. The first phase, which was repeated 5 times, consisted of

an apnea stage of 30 s, followed by a recovery phase of 60 s. The subjects were asked to perform apnea for 30 s, but were told to stop earlier if they were feeling extremely fatigued.
The second part, which was repeated for 5 times, included a deep respiration followed by a recovery phase of 60 s. During the deep respiration, the subject made a forced deep inspiration, followed by a deep expiration. The deep respiration did not have a predetermined duration, but it lasted according to the subject's capability. Once the protocol finished, the chest strap was first removed in those subjects who wore it, while the Holter was removed secondly.

4.3 DATA STRUCTURE

The data have been organized in a database, called 'Respiration Database'. It contains a file (.xlxs) called 'SubjectsData' and 50 datasets (MATLAB files), containing RSs acquired from the 50 subjects. SubjectsData.xlxs is an Excel file than includes clinical data and tests data of all subjects. The demographic data are sex ('M' = male or 'F' = female), age (years), height (cm), weight (kg), smoking attitudes ('YES' = smoker, 'NO' = no smoker, 'EX' = ex-smoker), sport history ('YES' = athlete, 'NO' = non-athlete, 'EX' = ex-athlete) and COVID-19 history ('YES' = the subject had tested positive to COVID-19 virus in the past, 'NO' = never tested positive to COVID-19 virus). Tests data are the date of the acquisition, the durations of each apnea and each deep respiration of the subject (in seconds). Moreover, some notes are reported on how the signals were reconstructed. Each dataset is named as S*n*, where *n* refers to the number of the subject, according to the Excel file. Each dataset contains one folder, named Holter.
The Holter folder contains ECG signals, recorded at a sampling frequency of 1000 Hz. The Holter folder consists of the three sub-folders relative to the three types of respiration, respectively apnea, deep and norm. Each sub-folder contains 5 MATLAB binary files (.mat) acquired during the type of respiration after which the sub-folder is named, where 'apnea, 'deep' and 'norm' stand for apnea phase, deep respiration phase and normal respiration, respectively. For instance, apnea sub-folder contains ECG recordings acquired during apnea stages. In particular, the binary MATLAB files in each sub-folder, beyond being named after the type of respiration, are also named with a number N, which represents the N^{th} respiration of that given type, with N = 1, … 5. In this way the 5 respirations are numbered in a chronological order. For instance, apnea3 is the ECG signal acquired during the 3^{rd} apnea. As a result, the Holter folder for each subject contains 15 binary MATLAB files in total. All

the binary MATLAB files are 30 s long. When the subject was not able to perform apnea for 30 s, some seconds of normal respiration following the apnea episode were included in the making of the 30 s ECG 'apnea' signal. Signals from normal respiration ('norm') have been obtained by considering the central window of the original ECG recording during normal respiration. Finally, 'deep' respiration signals were obtained by including, in the given order, some seconds prior to the deep respiration, the effective deep respiration and some seconds after the deep respiration episode, in order to make a 30 s ECG 'deep' signal, where the effective deep respiration lies in the central part of the signal.

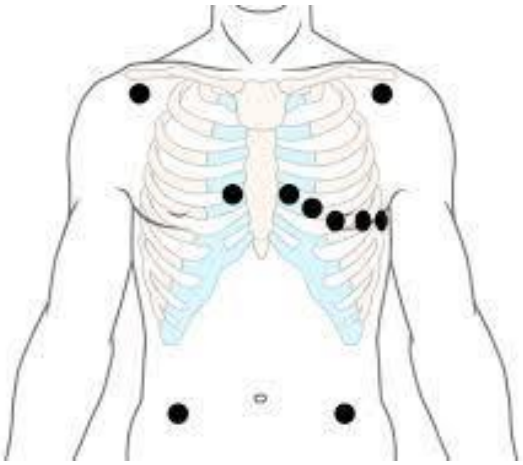

Figure 40. M-L configuration for electrodes positioning

5 NOVEL TECHNIQUE FOR THE EXTRACTION OF THE RESPIRATORY SIGNAL FROM THE ELECTROCARDIOGRAM

5.1 METHODS

In this chapter a novel technique is proposed for the estimation of respiratory patterns starting from ECG recordings. This method has been tested on the Respiration Database previously described. The working environment was MATLAB version 9.10.0 (R2021a).

5.1.1 Pre-processing

In the beginning, data were undersampled at 200 Hz, starting from an original sampling frequency of 1000 Hz. The signal was then filtered. In order to remove the HF components that are not related to respiration, a low-pass (LP) filter (6^{th} order, Butterworth filter) was used, with a cut-off frequency of 40 Hz. Afterwards, a QRS detector, such as Pan-Tompkins algorithm, was used to identify the R peaks and generate an R peak sequence [37].

5.1.2 Segmented-Beat Modulation Method for electrocardiogram derived respiration

SBMM aims at reconstructing a clean ECG from a noisy ECG recording. SBMM assumes that R peaks positions are known and that the ECG is made of the repetition of N cardiac cycles (CC), which may differ in terms of amplitude and duration. The CC onset is identified in the PQ segment Δt ms before the R peak. The SBMM hypothesizes that the QRS complex duration is constant within each cycle and does not vary with RR interval, whereas the duration of all other ECG waves varies linearly with it. Under this assumption, the CC can be divided into two segments, the QRS and the TUP. The QRS segment is determined $\pm\ \Delta$t ms around the R peak, while the TUP segment is identified Δt ms after the R peak and Δt ms before the next R peak. Every CC is considered to have its own amplitude and duration. However, in practical terms, the QRS segment has always the same duration in each CC and it is equal to twice Δt, whereas the TUP segment is variable and it is defined as the difference between the CC duration and the QRS duration (Fig. 41).

According to SBMM, CCs and the median RR interval (mRR) can be obtained by using the R-peak sequence from the noisy ECG. Before computing the mCC, all CCs, in particular only the TUP segments, are modulated either by linear stretching or modulation, in order to have their length

equal to mRR. The mCC is then obtained as the median of all CCs reconstructed by using the QRS segments with their original length and the modulated TUP segments.

Before concatenating N modulated mCCs, the TUP segment is demodulated by stretching or compression, in order to have its duration equal to the TUP segment duration of the corresponding CC in the noisy ECG. In the end, CCs are reconstructed and optimized to compensate for possible small inter-beat, nonlinear HR variations of CC waveforms. Last step is CC concatenation, that gives as output the clean ECG. It is worth mentioning that the output signal from SBMM does not have the same length as the original signal. In fact, SBMM provides an output signal that starts *d* seconds after the input, and ends *d* seconds before it, where *d* is a parameter that depends on the input. Fig. 42 summarizes all the steps of SBMM [1].

In order to extract EDR from the ECG, a mSBMM version was used. In fact, mSBMM does not include the optimization process for CCs. Optimization makes each extracted beat as similar as possible, in amplitude, to the other beats. Nevertheless, since the aim of this study was to identify respiratory patterns, hence, to analyze the ECG modulation induced by respiration, this step had been avoided. Fig. 43 is a block diagram of the mSBMM [2].

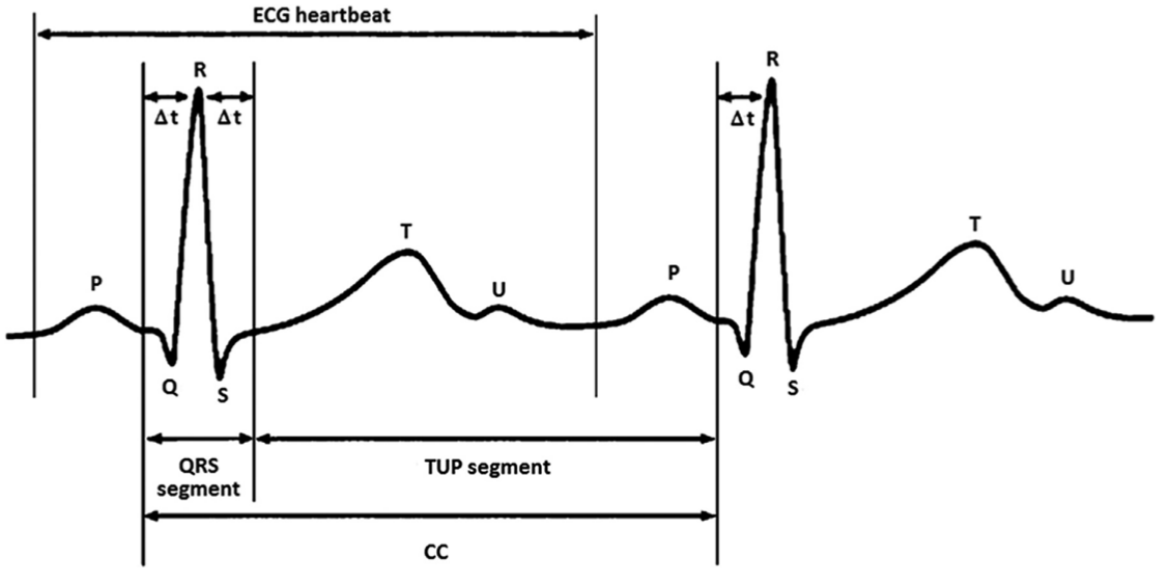

Figure 41. Typical ECG waveform, representing a specific CC, starting and ending at the beginning of the Q wave, segmented in QRS and TUP segments [1].

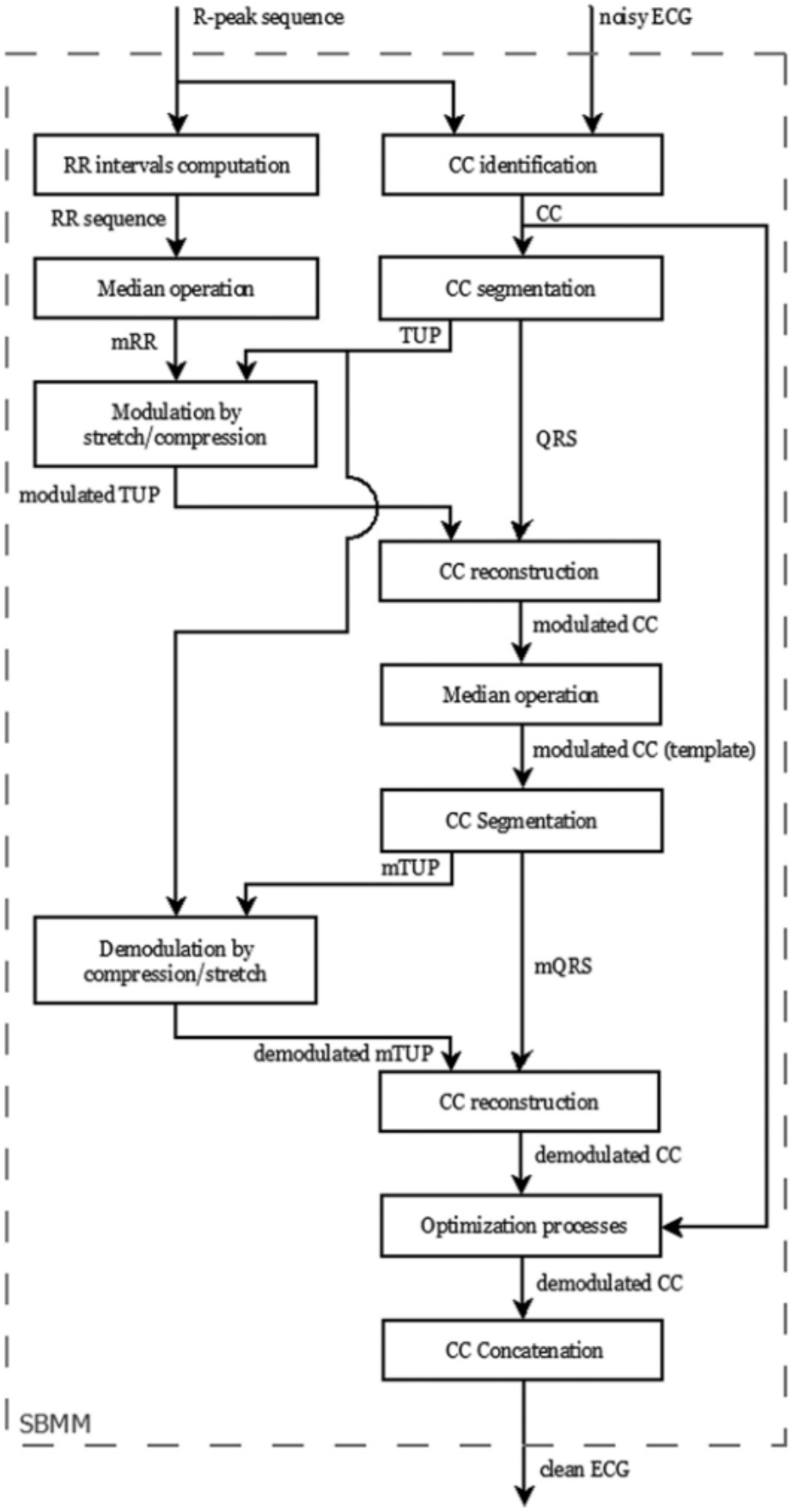

Figure 42. Block diagram of SBMM [1].

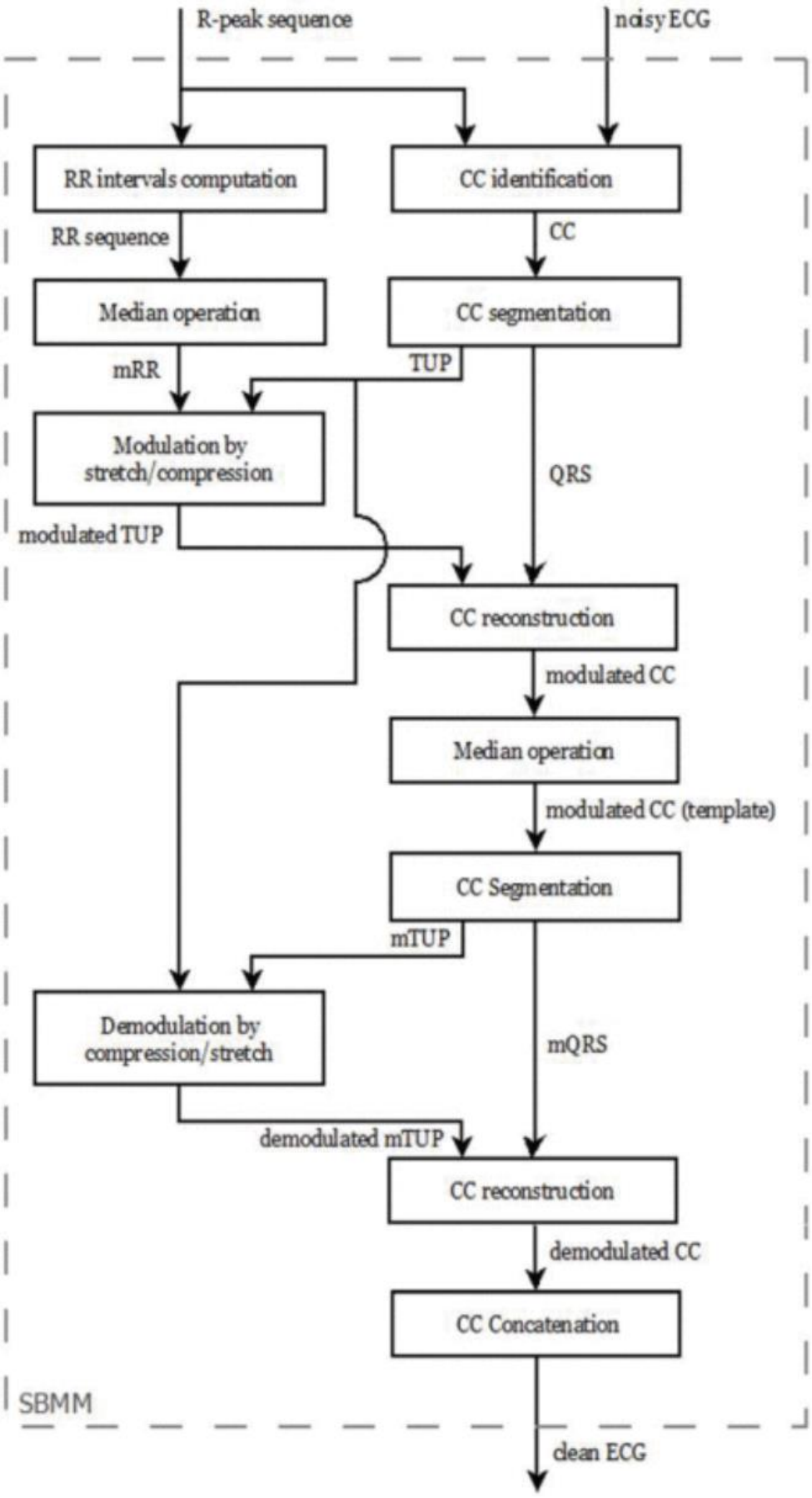

Figure 43. Block diagram of mSBMM [2].

Starting from the output of the mSBMM, a clean ECG not affected by respiration, EDR was retrieved, by means of subtraction between the original ECG, which is modulated by respiration, and the clean ECG. [2] Fig. 44 shows all the steps to obtain EDR. These steps were repeated across all the 50 subjects from the database, for ECG recordings from all 12 leads. Fig. 45 represents an example of EDR extraction.

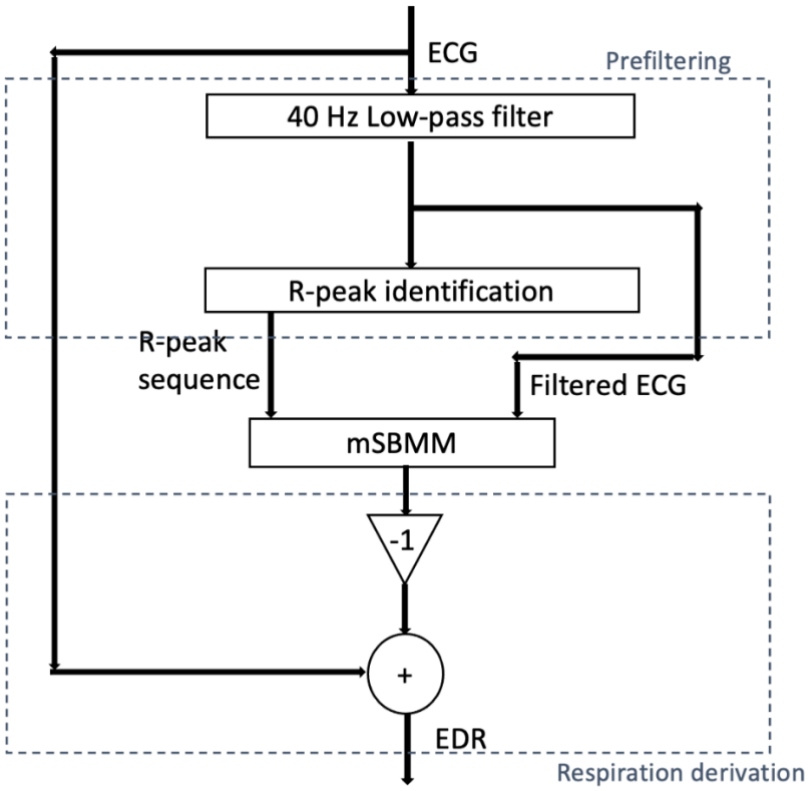

Figure 44. Block diagram summarizing all the steps for EDR extraction

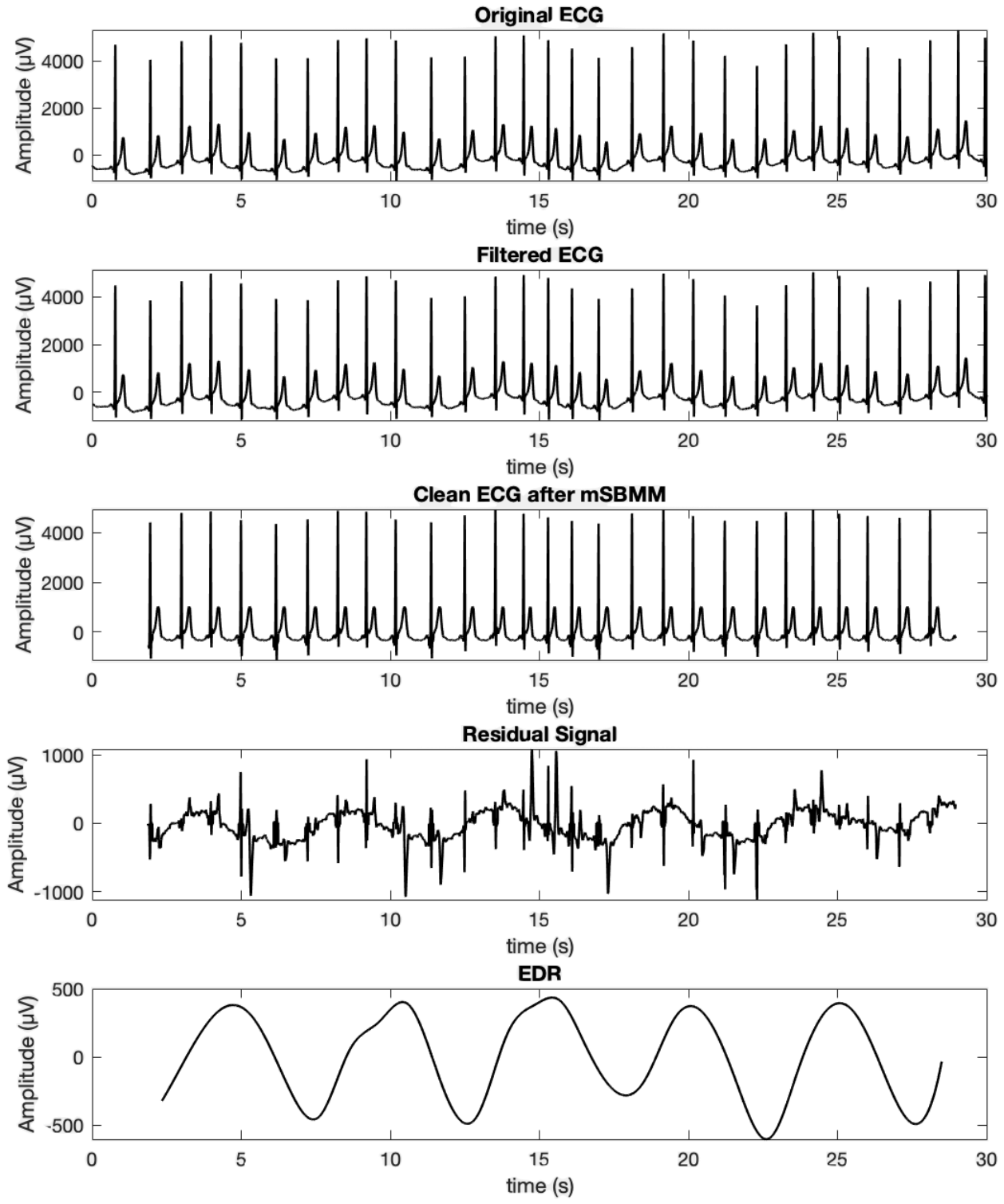

Figure 45. Steps for EDR extraction: original ECG undersampled at 200 Hz, filtered ECG, clean ECG after mSBMM application, residual signal defined as the difference between the input to mSBMM (filtered ECG) and output from mSBMM, EDR.

5.1.3 Amplitude characterization of the electrocardiogram derived respiration

Once EDR signals have been obtained, the amplitude of the signals has been computed, for each of the 50 subjects, from each lead, for each respiratory pattern,. Three methods have been used to quantify the amplitude, as represented in Fig. 46:

1. In the first method, the amplitude was obtained as the difference between the maximal and minimal values assumed by EDR signal.
2. The second method works under the assumption that the signal has zero mean and computes the amplitude as four times the standard deviation (SD) of the signal.
3. The third method does not assume a zero-mean signal, and computes the EDR amplitude as the difference between the 75^{th} percentile and the 25^{th} of the signal.

5.1.4 Statistics

After the amplitudes of EDR signals have been computed, their non-normal distributions have been estimated for each lead, across all the subjects, in terms of median (25^{th} percentile and 75^{th} percentile) values. The accuracy in estimating the respiration patterns has been assessed by means of the Wilcoxon paired signed rank test, which is a non-parametric statistical hypothesis test. The statistical test has been run on all the three methods used to quantify EDR signals, across each lead, comparing two types of respiration. Statistical significance was set at 0.05. In addition, the power of EDR amplitude to discriminate between different types of respiration, that is saying the diagnostic power of EDR amplitude, has been tested by means of the receiver operating characteristics (ROC) curve, especially by measuring the area under the curve (AUC). Significant results were set at AUC > 75%.

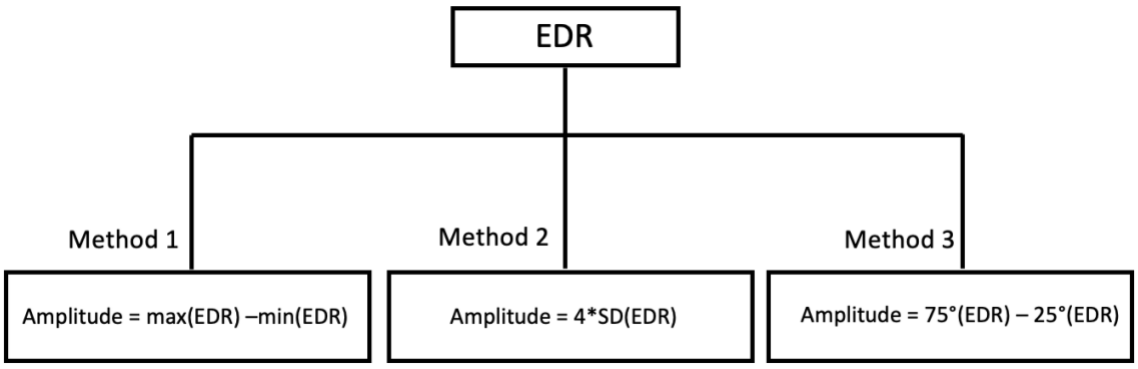

Figure 46. Amplitude characterization of EDR

5.2 RESULTS

In Table 7 the non-normal distributions of EDR amplitudes for each lead are reported, measured across all the subjects. Table 8 shows the result of the Wilcoxon paired signed rank test, whereas in Table 9 the values of the area under the ROC curve are indicated.

Table 7. Distributions of EDR amplitudes (mV) across all the subjects, for each ECG lead and for different types of respiration: median [25°; 75°]

	M1			M2			M3		
Lead	Apnea (µV)	Deep (µV)	Norm (µV)	Apnea (µV)	Deep (µV)	Norm (µV)	Apnea (µV)	Deep (µV)	Norm (µV)
I	189 [138;255]	358 [265;541]	265 [197;334]	170 [122;230]	326 [235;483]	227 [163;290]	58 [38;87]	102 [72;142]	82 [56;106]
II	698 [49;954]	822 [653;1172]	643 [496;859]	648 [439;851]	733 [566;1004]	574 [447;813]	209 [110;320]	249 [181;330]	200 [139;288]
III	689 [452;934]	878 [618;1245]	662 [460;851]	633 [415;836]	766 [545;1059]	566 [412;792]	212 [129;306]	240 [176;359]	196 [139;288]
aVR	410 [283;558]	481 [365;631]	396 [314;526]	362 [244;492]	410 [313;551]	364 [263;484]	109 [63;175]	132 [95;196]	118 [78;176]
aVL	352 [211;469	504 [368;665]	351 [245;480]	320 [189;420]	437 [317;599]	325.51 [228;444]	108 [61;162]	134 [93;189]	111 [76;168]
aVF	698 [450;962]	863 [653;1161]	610 [469;850]	641 [413;858]	791 [563;1029]	539 [399;824]	218 [127;318]	264 [180;371]	186 [130;309]
V1	578 [419;820]	797 [615;1085]	697 [485;924]	533 [374;714]	722 [55;987]	636 [448;864]	181 [124;250]	258 [184;346]	227 [163;328]
V2	769 [556;1114]	1341 [938;1688]	1058 [777;1373]	749 [493;1035]	1221 [859;1563]	1002 [711;1285]	267 [176;375]	406 [317;555]	357 [246;493]
V3	832 [662;1118]	1234 [979;1606]	949 [701;1177]	756 [549;1045]	1084 [856;1434]	835 [633;1070]	264 [189;383]	353 [262;438]	301 [233;405]
V4	679 [448;1008]	1222 [901;1999]	676 [493;1103]	581 [378;855]	1125 [786;1729]	602 [455;982]	196 [113;310]	297 [214;466]	227 [152;333]
V5	668 [449;932]	1254 [899;1956]	717 [531;1017]	554 [378;790]	1119 [800;1836]	612 [444;898]	176 [101;266]	310 [188;476]	209 [135;318]
V6	340 [197;569]	976 [713;1385]	514 [305;782]	316 [161;495]	909 [654;1414]	488 [289;731]	89 [48;166]	256 [158;400]	190 [99;278]

Table 8. p values from Wilcoxon paired signed rank test. Green boxes represent statistically significant results.

	M1			M2			M3		
Lead	A vs D	A vs N	D vs N	A vs D	A vs N	D vs N	A vs D	A vs N	D vs N
I	10^{-39}	10^{-18}	10^{-31}	10^{-38}	10^{-17}	10^{-33}	10^{-29}	10^{-16}	10^{-15}
II	10^{-11}	0.37	10^{-18}	10^{-07}	0.31	10^{-14}	10^{-04}	0.53	10^{-08}
III	10^{-12}	0.08	10^{-21}	10^{-10}	0.11	10^{-19}	10^{-03}	0.48	10^{-10}
aVR	10^{-09}	0.66	10^{-11}	10^{-06}	0.78	10^{-07}	10^{-04}	0.67	10^{-03}
aVL	10^{-24}	0.15	10^{-26}	10^{-24}	0.02	10^{-24}	10^{-12}	10^{-03}	10^{-09}
aVF	10^{-13}	0.05	10^{-23}	10^{-09}	0.07	10^{-21}	10^{-05}	0.16	10^{-12}
V1	10^{-17}	10^{-04}	10^{-15}	10^{-20}	10^{-07}	10^{-13}	10^{-17}	10^{-10}	10^{-04}
V2	10^{-36}	10^{-19}	10^{-30}	10^{-34}	10^{-20}	10^{-27}	10^{-26}	10^{-16}	10^{-13}
V3	10^{-26}	0.04	10^{-25}	10^{-24}	0.02	10^{-21}	10^{-13}	10^{-04}	10^{-07}
V4	10^{-34}	0.01	10^{-33}	10^{-35}	10^{-03}	10^{-34}	10^{-22}	10^{-04}	10^{-13}
V5	10^{-39}	10^{-05}	10^{-33}	10^{-37}	10^{-04}	10^{-35}	10^{-20}	10^{-04}	10^{-16}
V6	10^{-41}	10^{-18}	10^{-35}	10^{-41}	10^{-23}	10^{-38}	10^{-34}	10^{-21}	10^{-15}

Table 9. Area Under the Curve (AUC) from ROC curve. Green boxes highlight AUC values greater than 75%.

	M1			M2			M3		
Lead	A vs D	A vs N	D vs N	A vs D	A vs N	D vs N	A vs D	A vs N	D vs N
I	83%	68%	71%	81%	66%	71%	77%	67%	64%
II	63%	48%	67%	61%	48%	65%	60%	50%	61%
III	65%	47%	69%	65%	47%	68%	59%	49%	61%
aVR	62%	50%	62%	60%	51%	59%	59%	54%	56%
aVL	72%	52%	71%	71%	54%	69%	64%	55%	59%
aVF	64%	46%	70%	63%	46%	68%	60%	49%	63%
V1	68%	58%	61%	70%	61%	60%	70%	64%	56%
V2	79%	67%	66%	78%	67%	64%	75%	66%	59%
V3	76%	55%	72%	74%	56%	70%	65%	58%	59%
V4	80%	53%	77%	81%	56%	77%	72%	58%	66%
V5	83%	57%	78%	83%	57%	79%	72%	58%	66%
V6	90%	65%	80%	90%	68%	80%	83%	72%	64%

5.3 DISCUSSION

The aim of this study is to characterize EDR in terms of amplitude, in a way that different types of respiration can be classified according to EDR amplitude. The study has been carried out on a database in which the subjects performed three different types of respiration, including apnea, deep respiration and normal respiration. Three methods have been used to estimate EDR amplitude. By analyzing the results, it can be appreciated that all the three methods led to statistically significant outcomes. This confirms that the amplitude characterization of respiration is efficient and provides a valid alternative to BB interval measurements. For all three methods, it has been observed that the EDR relative to deep respiration has a median amplitude that is higher than the one from normal respiration and from apnea. This confirms the discriminating power of EDR amplitude when comparing deep respiration with other types of respiration. On the other hand, when comparing apnea with normal respiration, in some leads the median EDR amplitude of apnea is much lower than the one from normal respiration. However, in other leads this difference in amplitude is very small, or even it happens that apnea has a greater amplitude than normal respiration. This is then reflected in the results from Wilcoxon paired test. In fact, comparing deep respiration with either apnea or normal respiration always gives statistically significant results, for all three methods. On the other hand, when considering the case 'apnea vs normal respiration', some leads are characterized by statistically significant results, while others are not. This has especially occurred in leads II, III, aVR and aVF for all three methods, in addition to lead aVL when using the first method. Hence, even though apnea is physiologically different from normal respiration, it may happen that the ECG modulation is very similar for both apnea and normal respiration. Moreover, even though apnea is the cessation of breathing, not all people pass from a normal respiration to an apnea phase in the same way. There are in fact people who start an apnea stage by taking a deep breath prior to apnea, but also some who do not take a deep breath. This contributes to variability in the signals relative to apnea, and can in turn corrupt the amplitude characterization. Furthermore, the database has been reconstructed by considering 30 s-long signals. However, some subjects could hardly hold apnea during this period, and were feeling fatigued. This may have consequences on the autonomic control on the cardiac activity, and thus interfere with ECG modulation typical of apnea.

Considering the diagnostic power of EDR classification from ROC test, it can be appreciated that the first method achieved the best results. In particular, an AUC greater than 75% was found in lead I, and from V2 to V6 when comparing apnea with deep respiration, whereas only leads V4 to V6

provided good results when analyzing deep respiration vs normal. Nevertheless, no good results have been found when comparing apnea with normal respiration. This is probably resulting from the minimal differences in amplitude between apnea and normal respiration. Moreover, the reasons behind this are not clear yet, and must be properly investigated, in particular it should be analyzed the influence of the autonomic nervous system on the cardiac activity during apnea. In general, it can be stated that the good performance of this method is likely caused by the fact that the data have been preprocessed in order to remove the noise, in a way that it is highly likely that the maxima and minima have been correctly detected. It must be underlined that this method cannot be applied to every context. Thinking for instance of wearable devices, amplitude characterization in terms of maxima and minima is not always reliable. Indeed, wearable sensors are very sensitive to noise, which in turn can corrupt the identification of maxima and minima. Consequently, unless a preprocessing filter stage is implemented in the wearable device, statistical techniques should be used to estimate the amplitude.

Considering the second and third method, the latter showed the worst results, having an AUC greater than 75% only in lead I and V6, for the case apnea vs deep respiration. On the other side, the second method showed a satisfying performance, when comparing deep respiration with other types of respiration. In particular, the best results were obtained when comparing deep respiration with apnea, finding an AUC greater than 75% in leads I, V2, and from V4 to V6. However, as it was for the first method, no good results were found for the case apnea vs normal respiration. The reason why these last two methods show such differences in their performance lies right in the way EDR amplitude was estimated. As a matter of fact, when using the second method, that is saying computing EDR amplitude as four times the SD of EDR, the tail of the distribution is neglected by definition of how the parameter is characterized, and only the signal around the mean $\pm$ SD is analyzed. As a result, the two signals to be compared are dissimilar, and diagnostic power of the second method is high. On the other hand, when computing EDR amplitude in the interquartile range, as the third method does, the tails of the signal are counted. As a consequence, unbalanced tails appear, and some underestimation may happen. In this way, the third method hardly discriminates between different types of respiration, leading to a low diagnostic power. This suggests that, when the choice for amplitude characterization is between statistical techniques, as the second and third method are, the second one results to be the most suitable. It is necessary to stress out that, in general, an AUC greater than 75% has been found in some of the precordial leads, beyond lead I. This may be related to the mechanical movement of heart and diaphragm during respiration that

contribute to ECG modulation. This movement can in fact be sensed the most on the thorax, that is the place of precordial leads.

CONCLUSION

The aim of this study is to characterize EDR in terms of amplitude, in order to provide a valid alternative to BB interval measurement of the RS, which are not always able to correctly classify different types of respiration . Three methods have been used to characterize EDR amplitude. Among these, all were able to correctly classify deep respiration when compared to apnea or normal respiration. Nevertheless, when considering the classification of apnea with respect to normal respiration, statistically significant results were obtained only for some leads, in all methods. Hence, future studies could be conducted investigating the classification of apnea vs normal respiration, in terms of amplitude. Among the three methods for EDR amplitude characterization, the first one, which measures the amplitude as the difference between the maximum and minimum of the signal, proved to be the most statistically significant. However, this method can only be applied to filtered signals, hence suitable alternatives should be used to characterize noisy EDRs, such as statistical techniques. Among the two statistical techniques which were tested in this study, one involving SD and the other one employing the interquartile range, only the first one provided statistically significant results. Hence, future studies could be conducted to investigate the effects of EDR characterization by means of interquartile range. Furthermore, additional studies could be carried out to exploit the Respiration Database. In fact, the database is composed of data obtained from an Holter device and a chest strap. However, in this study only data from Holter device have been used. Therefore, future studies could be performed including also data from the chest strap, which can provide a direct measurement of some respiratory parameters. In conclusion, based on the results, it can be stated that amplitude characterization of EDR is a valid alternative to BB measurements, since it allows to distinguish between different types of respiration.

BIBLIOGRAPHY

[1] A. Agostinelli, A. Sbrollini, C. Giuliani, S. Fioretti, F. Di Nardo and L. Burattini, "Segmented beat modulation method for electrocardiogram estimation from noisy recordings," *Medical Engineering and Physics,* vol. 38, pp. 560-568, 2016.

[2] B. Pambianco, A. Sbrollini, I. Marcantoni, M. Morettini, S. Fioretti and L. Burattini, "Electrocardiogram Derived Respiratory Signal through the Segmented-Beat Modulation Method," in *2018 40th Annual International Conference of the IEEE Engineering in Medicine and Biology Society. IEEE Engineering in Medicine and Biology Society. Annual Conference*, 2018.

[3] G. Ambrosi, P. Castano and R. F. Donato, Anatomia dell'uomo, seconda edizione, Edi. Ermes, 2006.

[4] G. van der Bie, Anatomy, Morhological Anatomy from a Phenomenological Point of View, Louis Bolk Institute, 2012.

[5] W. Boron and E. L. Boulpaep, Medical Physiology, third edition, Elsevier, 2016.

[6] G. Hedenstierna and J. B. Borges, "Normal physiology of the respiratory system," in *Oxford Textbook of Critical Care, second edition*, Oxford University Press, 2019, pp. 1-6.

[7] R. Klabunde, Cardiovascular Physiology Concepts, second edition, Lippincott Williams & Wilkins, 2011.

[8] Harvard Medical School, "Harvard Health Publishing," 6 July 2020. [Online]. Available: https://www.health.harvard.edu/mind-and-mood/relaxation-techniques-breath-control-helps-quell-errant-stress-response.

[9] L. Whited and D. D. Graham, "StatPearls - NCBI Bookshelf," 26 July 2021. [Online]. Available: https://www.ncbi.nlm.nih.gov/books/NBK470309/.

[10] G. G. Mazeika, M. R. Swanson and C. RPSGT, "Respiratory Inductance Plethysmography An Introduction," *Pro-Tech Services, Inc.,* pp. 4-5, 2007.

[11] J.-H. Kim, R. Roberge, J. B. Powell, A. B. Shafer and W. Jon Williams, "Measurement Accuracy of Heart Rate and Respiratory Rate during Graded Exercise and Sustained Exercise in the Heat Using the Zephyr BioHarnessTM," *Int J Sports Med.,* vol. 34, no. 6, pp. 497-501, 2013.

[12] G. Gutierrez and V. K. Jain, "Respiratory Inductance Plethysmography Improved Diagnostic Sensitivity and Specificity of Obstructive Sleep Apnea," *Respiratory Care,* vol. 61, no. 8, pp. 1033-1037, 2016.

[13] J. J. Goldberger and J. Ng, Practical Signal and Image Processing in Clinical Cardiology, Springer, 2010.

[14] F. P. Branca, Fondamenti di Ingegneria Clinica - Volume 1 (Italian Edition), Springer, 2000.

[15] P. Palatini, "Need for a Revision of the Normal Limits of Resting Heart Rate," *American Heart Association,* vol. 33, no. 2, pp. 622-625, 1999.

[16] Institute for Quality and Efficiency in Health Care, "InformedHealth.org - NCBI Bookshelf," 31 January 2019. [Online]. Available: https://www.ncbi.nlm.nih.gov/books/NBK536878/.

[17] J. Feher, The Heart as a Pump, Second Edition, ACADEMIC PRESS, 2012.

[18] P. H. Charlton, D. A. Birrenkott, T. Bonnici, M. A. F. Pimentel, A. E. W. Johnson, J. Alastruey, L. Tarassenko, P. J. Watkinson, R. Beale and D. A. Clifton, "Breathing Rate Estimation From the Electrocardiogram and Photoplethysmogram," *IEEE Reviews in Biomedical Engineering,* vol. 11, pp. 2-20, 2018.

[19] S. Kurisu, K. Nitta, Y. Sumimoto, H. Ikenaga, K. Ishibashi, Y. Fukuda and Y. Kihara, "Effects of deep inspiration on QRS axis, T-wave axis and frontal QRS-T angle in the routine electrocardiogram," *Heart and Vessels,* vol. 34, pp. 1519-1523, 2019.

[20] J. Pucik, M. Uhrìk, A. Sultan and J. Šurda, "Experimental Setup for Cardio-Respiratory Interaction Study," in *Trends in Biomedical Engineering: Proceedings of the 8th Czech-Slovak Conference*, Bratislava, 2009.

[21] R. Bailon, L. Sornmo and P. Laguna, "ECG-derived respiratory frequency estimation," in *Advanced Methods and Tools for ECG Data Analysis*, Artech House, 2006.

[22] L. Bacharova, E. Triantafyllou, C. Vazaios, I. Tomeckova, I. Paranicova and R. Tkacova, "The effect of obstructive sleep apnea on QRS complex morphology," *Journal of Electrocardiology,* vol. 48, no. 2, pp. 164-170, 2015.

[23] D. Labate, F. La Foresta, G. Occhiuto, F. C. Morabito, A. Lay-Ekuakille and P. Vergallo, "Empirical Mode Decomposition vs. Wavelet Decomposition for the Extraction of Respiratory Signal from Single-Channel ECG: A Comparison," *IEEE SENSORS JOURNAL,* vol. 13, no. 7, pp. 2666-2674, 2013.

[24] S. Mallat, A Wavelet Tour of Signal Processing, Vols. New York, NY, USA: Academic Press, New York, NY, USA: Academic Press, 1999.

[25] N. E. Huang, Z. Shen, S. R. Long, M. C. Wu, H. H. Shih, Q. Zheng, N. C. Yen, C. C. Tung and H. H. Liu, "The empirical mode decomposition and the Hilbert spectrum for non-linear and non stationary time series analysis," *Proc Royal Soc. London A,* vol. 454, pp. 903-995, 1998.

[26] M. Campolo, D. Labate, F. La Foresta, F. C. Morabito, A. Lay-Ekuakille and P. Vergallo, "ECG-Derived Respiratory Signal using Empirical Mode Decomposition," in *2011 IEEE International Symposium on Medical Measurements and Applications*, 2011.

[27] W. Einthoven, G. Fahr and A. de Waart, "On the direction and manifest size of the variations of potential in the human heart and on the influence of the position of the heart on the form of the electrocardiogram," vol. 40, no. 2, pp. 163-211, 1950.

[28] E. Helfebein, R. Firoozabadi, S. Chien, E. Carlson and S. Babaeizadeh, "Development of three methods for extracting respiration from the surface ECG: a review," *Journal of Electrocardiography,* vol. 47, pp. 819-825, 2014.

[29] Z. B. Khaled and G. Farges, "First approach for respiratory monitoring by amplitude demodulation of the electrocardiogram," in *1992 14th Annual International Conference of the IEEE Engineering in Medicine and Biology Society*, Paris, 1992.

[30] G. B. Moody, R. G. Mark, A. Zoccola and S. Mantero, "Derivation of Respiratory Signals from Multi-lead ECGs," *Computers un Cardiology,* vol. 12, pp. 113-116, 1985.

[31] J. Lázaro, A. Alcaine, D. Romero, E. Gil, P. Laguna, E. Pueyo and R. Bailón, "Electrocardiogram Derived Respiratory Rate from QRS Slopes and R-Wave Angle," *Annals of Biomedical Engineering,* vol. 40, no. 10, pp. 2072-2083, October 2014.

[32] E. Pueyo, L. Sormno and P. Laguna, "QRS slopes for detection and characterization of myocardial ischemia," *IEEE Trans. Biomed. Eng.,* vol. 55, no. 2, pp. 468-477, 2008.

[33] H. L. Chan, S. H. Lin, F. T. Wang, W. Y. Hsu and C. L. Wang, "ECG-derived respirations based on phase-space reconstruction of single-lead ECG: Validations over various physical activities based on parallel recordings of ECG, respiration, and body accelerations," in *2014 36th Annual International Conference of the IEEE Engineering in Medicine and Biology Society*, 2014.

[34] H. Sharma and K. K. Sharma, "Application of iterated Hilbert transform for deriving respiratory signal from single-lead ECG," in *2016 1st India International Conference on Information Processing (IICIP)*, 2016.

[35] [Online]. Available: www.globalinstrumentation.com.

[36] [Online]. Available: https://www.zephyranywhere.com/media/download/bioharness3-user-manual.pdf.

[37] J. Pan. and W. J. Tompkins, "A Real-Time QRS Detection Algorithm,," *IEEE Transactions on Biomedical Engineering,* Vols. BME-32, no. 3, pp. 230-236, 1985.